Available online at www.sciencedirect.com
ScienceDirect
Precambrian Research 156 (2007) 195–225
Precambrian Research
www.elsevier.com/locate/precamres

U–Pb and Hf-isotope analyses of zircon from the Kundelungu Kimberlites, D.R. Congo: Implications for crustal evolution

J.M. Batumike [a,b,*], S.Y. O'Reilly [a], W.L. Griffin [a], E.A. Belousova [a]

[a] *ARC National Key Centre for Geochemical Evolution and Metallogeny of Continents, Department of Earth and Planetary Sciences, Macquarie University, NSW 2109, Australia*

[b] *Université de Lubumbashi, Département de Géologie, B.P. 1825, Lubumbashi, Congo*

Received 15 December 2006; received in revised form 2 April 2007; accepted 4 April 2007

Abstract

The Gungwania and Talala kimberlitic pipes on the Kundelungu Plateau (Katanga, SE Congo) have been used as drillholes, to obtain crustal zircons for a study of crustal evolution in the region and to constrain the age of the basement and the sedimentary provenance of the Katangan Supergroup. Two hundred and twenty-nine zircon grains were analysed for U–Pb ages and Hf-isotope compositions. Juvenile Mesoarchean (~3.4–3.3 Ga) crust in the region underwent recycling during Neoarchean and Paleoproterozoic time. The Paleoproterozoic event involved little production of juvenile crust, and this Paleoproterozoic crust was recycled during Mesoproterozoic and Neoproterozoic time. Both the Mesoproterozoic and Neoproterozoic were characterised by bimodal magmatism reflecting extension, linked with the break up of Rodinia and the opening of the Katangan basin, and the development of juvenile crust. Detailed studies of the external morphology of the zircons in different age groups suggest that the basement beneath the Kundelungu region is predominantly Paleoproterozoic in age; other zircon populations may be derived from the Katangan sediments. The absence of any zircons younger than 560 Ma supports deposition of the Biano Subgroup, which hosts the kimberlites, during the Pan-African Lufilian orogeny. The Archean Congo and Zimbabwe cratons, the Paleoproterozoic Ubendian Belt (Bangweulu Block), the Paleo-to-Mesoproterozoic Irumide Belt, the Mesoproterozoic Kibaran Belt and the Choma Kalomo Block may all have contributed material to the sediments of the Katangan Supergroup.
© 2007 Elsevier B.V. All rights reserved.

Keywords: Zircon geochronology; Zircon U–Pb dating; Zircon Hf-isotopes; Crust evolution; Congo Craton; Kundelungu Kimberlite

1. Introduction

The Kundelungu Plateau consists of rocks belonging to the Katangan Supergroup, deposited during or after the Lufilian orogeny in late Neoproterozoic and early Paleozoic time. Sandstones intercalated with limestones, dolomites and mudrocks crop out on this Plateau, forming the Biano Subgroup at the top of the Katangan Supergroup (François, 1973, 1987; Batumike et al., 2007). The relative ages of these rocks and the location of the Kundelungu Plateau provide an opportunity to study the broad evolution of the Precambrian crust of the entire region, as the sediments were derived from the surrounding basement (Master et al., 2005; Batumike et al., 2006). Batumike et al. (2006) concluded that the Nguba and Kundelungu Group sediments were derived mainly from the Paleoproterozoic Bangweulu Block, the Paleo-to-Mesoproterozoic Irumide Belt and

* Corresponding author at: ARC National Key Centre for Geochemical Evolution and Metallogeny of Continents, Department of Earth and Planetary Sciences, Macquarie University, NSW 2109, Australia. Tel.: +61 2 9850 9676; fax: +61 2 9850 6904.
E-mail address: jbatumike@els.mq.edu.au (J.M. Batumike).

0301-9268/$ – see front matter © 2007 Elsevier B.V. All rights reserved.
doi:10.1016/j.precamres.2007.04.002

the Mesoproterozoic Kibaran Belt, with little contribution from the Neoarchean Congo-Kasai Craton. The Biano Subgroup also received sediments from the underlying Roan, Nguba and Kundelungu rocks as it was deposited in the Katangan foreland basin. However, the age and origin of the basement beneath the basin is controversial.

The presence of Mesoarchean xenocrystic and detrital zircon populations in Muva quartzites and Katangan volcanic lapilli (Rainaud et al., 2003) has been interpreted as evidence of a Mesoarchean basement beneath the Lufilian Belt. Master et al. (2005), based on $^{40}Ar/^{39}Ar$ ages of detrital muscovite from the Biano Subgroup sandstones, concluded that the minimum sedimentation age for the Katangan basin is 570 ± 5 Ma, implying that the Katangan Supergroup is mostly Neoproterozoic.

The development of in situ U–Pb laser ablation microprobe inductively coupled plasma mass spectrometer (LAM-ICPMS) dating allows the rapid determination of high quality age data on single zircon grains (e.g. Belousova et al., 2001; Jackson et al., 2004). Hf-isotope analysis by multi-collector (MC)-LAM-ICPMS on the same zircon grains provides additional information on the sources of their host magmas, and the determination of a model age for the parent rock (Griffin et al., 2000). Belousova et al. (2002) and Griffin et al. (2004) introduced a method for the recognition of the host parent rocks for zircons, based on their trace-element compositions. The combination of U–Pb ages, Hf-isotopes and trace elements on zircons from a specific geological region may then be used to develop a broad understanding of the evolution of the crust (e.g. O'Reilly et al., 2004).

This study is based on the analysis of zircons separated from heavy-mineral concentrates collected in drainages crosscutting the Gungwania and Talala kimberlite pipes in the Kundelungu Plateau (Gungwana River and Talala River, respectively). The zircons are xenocrysts in the kimberlites, derived from the underlying basement and from the Biano Subgroup sedimentary rocks (mostly sandstones) intruded by the kimberlites. In situ analysis of U–Pb ages, Hf-isotopes and trace-element patterns in the zircons have been used to investigate the evolution of the crust in the southeastern part of the Democratic Republic of the Congo (hereafter Congo), with implications for the surrounding areas. These data help to constrain the age and nature of the basement beneath the Kundelungu region, and the source rocks and the depositional age of the Katangan Supergroup, and provide new insights on tectonic events in the region.

2. Geological setting

The Kundelungu Plateau is located approximately 200 km north of Lubumbashi city, in SE Congo (Fig. 1). It constitutes the subhorizontal part of the Katangan Belt in its northern extension, known as the "tabular Katangan" contrasting with the folded referred to as the Lufilian Belt. The Katangan belt is surrounded by the Kibaran orogenic Belt to the northwest, the Bangweulu Block to the northeast and the Irumide Belt to the southeast. Further south, the basement rocks of the Zimbabwe Craton are exposed and to the west and northwest lies the Congo-Kasai Craton (Fig. 1). The Kibaran belt was formed during the Kibaran orogeny in Mesoproterozoic times. The Irumide Belt includes rocks of Paleoproterozoic and Mesoproterozoic ages. The Bangweulu Block formed during the Paleoproterozoic Ubendian orogeny, but may have older protoliths. The Congo-Kasai Craton includes mostly rocks of Meso-to-Neo-archean age similar to those in the Zimbabwe and Tanzania cratons.

2.1. Archean Congo-Kasai Craton

The Congo-Kasai Craton lies in the central part of the Congo (Kasai Province) and extends southward into Angola and northward into the Central Africa Republic, Gabon and Cameroon. However, correlation between the southern part of the craton (Angola-Kasai) and the northern extension is hampered by the thick Phanerozoic cover forming the "Cuvette Centrale". In the central part of Congo, it consists of granulite, gneiss, granite and amphibolite, a gabbro-noritic and gabbro-charnockitic complex, and a migmatitic complex. Age data for the Congo-Kasai Craton is sparse and largely comprised of old whole-rock Rb–Sr data. Delhal and Ledent (1973) reported a 3487 ± 67 Ma (Rb–Sr) model age (relative to bulk earth) on microcline from coarse-grained pegmatite of the "Haute-Lwanyi gneisses". Delhal and Liégeois (1982) reported a Rb–Sr whole-rock errorchron of 2852 ± 46 Ma for the Sandoa-Kapanga complex gneiss. Walraven and Rumvegeri (1993) found two different Pb–Pb errorchron ages in the Sandoa-Kapanga complex, 3086 Ma and 3021 ± 48 Ma. They interpreted these ages as representing two different metamorphic and tectonic events, D1 and D2, respectively, within the Congo-Kasai Craton. The later event was locally associated with anatectic melting and the production of granitoid magmas.

Sm–Nd and Rb–Sr isochron ages range between ~2.8 and 2.9 Ga in the northern part of the Congo Craton (e.g. Ntem complex) where

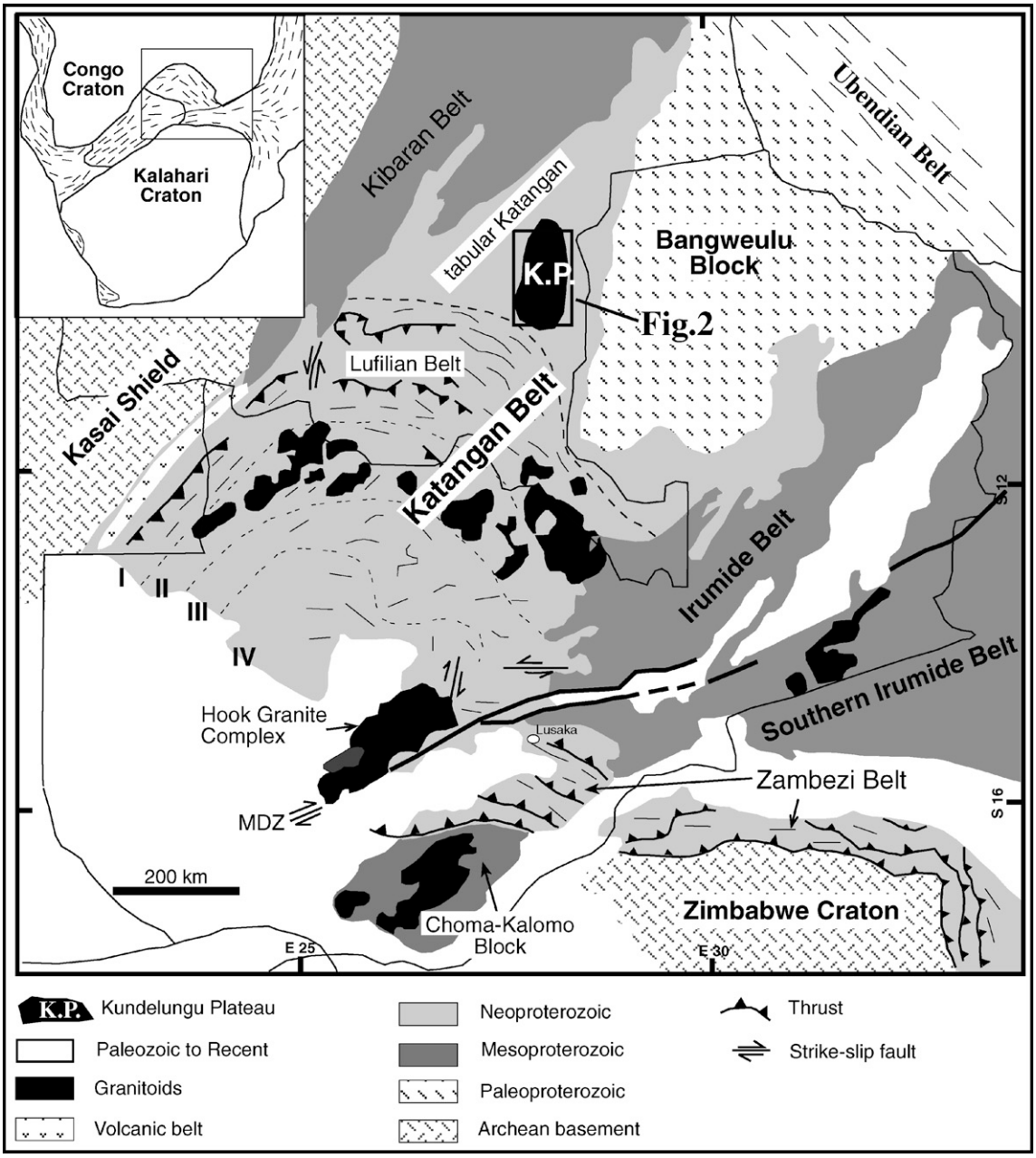

Fig. 1. Simplified geological map of the Katangan belt and surrounding basements (modified after Binda and Porada, 1995) and the location of the Kundelungu Plateau.

tonalite–trondhjemite–granodiorite (TTG) suites occur (Tchameni et al., 2000; Shang et al., 2004). Shang et al. (2004) suggested that these rocks crystallised from a late Mesoarchean crust (>2.9 to ~3.2 Ga), based on Nd model ages. The late magmatic event in the Congo-Kasai Craton is represented by late granitoids observed in both parts of the craton, including K-rich granite from northern Gabon (2637 ± 33 Ma; whole-rock Rb/Sr; Tchameni et al., 2000) and from the Chaillu area in southern Gabon (2678 ± 23 Ma; whole-rock Rb/Sr; Caen-Vachette et al., 1988), and the Malafundi granites from the Dibaya complex in Congo (2648 ± 22 Ma; Rb/Sr; Delhal et al., 1976). Within this late complex a youngest age of 2595 ± 92 Ma (Rb/Sr, MSWD = 0.86) was reported by Cahen et al. (1984). However, this age has a large uncertainty and is within error of that

published by Delhal et al. (1976). Further south of the craton in NW Zambia, Key et al. (2001) found ages between 2540 and 2560 Ma (SHRIMP U–Pb zircon) in a suite of metamorphic and igneous rocks of the Kasai Shield.

2.2. Paleoproterozoic basement

The Paleoproterozoic Ubendian Belt (defined at Ubende in Tanzania) extends from Tanzania to Mozambique and the Congo. Three major deformation events are recognised in Tanzania (Lenoir et al., 1994). The first event, isotopically dated at 2100–2025 Ma, is interpreted as a collisional event that created the belt (Lenoir et al., 1994). The second deformational phase is represented by late-to-post-kinematic calc-alkaline granitic batholiths dated at ca. 1860 Ma, but locally reactivated around ca. 1725 Ma. A late third deformation event in the Ubendian Belt is of Neoproterozoic age (ca. 750 Ma) and is characterised by the presence of alkaline plutons (Lenoir et al., 1994).

Kabengele et al. (1991) described similar potassic calc-alkaline magmatism in the Pepa-Lubumba area (NE Katanga, Congo) that was dated at 1861 ± 28 Ma (Rb/Sr isochron; Kabengele et al., 1991). The Bangweulu Block in Zambia includes terranes ranging in age between 1950 and 1800 Ma (Vrána et al., 2004). These terranes include the Mkushi gneiss (N'Gambi et al., 1986) and some granitic domes inside the copperbelt (Kabompo dome, Key et al., 2001; Kafue dome, Rainaud et al., 1999; Luina granite, Ngoyi et al., 1991).

De Waele et al. (2006a), using whole-rock geochemistry and Sr–Nd isotopic data on granitoids and volcanic rocks from the Bangweulu Block and Irumide Belt of Zambia, recognised four main igneous events, named the Usagaran phase (2.05–1.93 Ga), the Ubendian phase (1.88–1.85 Ga), the Lukamfwa phase (1.65–1.55 Ga) and the Irumide phase (1.05–0.95 Ga). According to these authors, the T_{DM} model ages of 3.3–2.8 Ga for granitoids and 2.9–2.4 Ga for volcanic rocks indicate the presence of a preponderant Archean crust within the Bangweulu Block and within the Irumide Belt. They suggested that during these periods there was little input of juvenile mantle-derived material (De Waele et al., 2006a). The two first events defined by De Waele et al. (2006a) in Zambia are correlative with the two main Paleoproterozoic events in the Ubendian Belt in Tanzania (Lenoir et al., 1994) and the cratonic collisional events that could have led to the formation of a Paleoproterozoic supercontinent as postulated by Condie (2002), among others.

2.3. Mesoproterozoic basement

Three main Mesoproterozoic areas are known in the region: the Kibaran (Congo) and the Irumide (Zambia) Belts and the Choma-Kalomo Block (Fig. 1). Cahen et al. (1984) defined four major granitoid groups within the Kibaran Belt: (1) type A or G_1 granitoids with Rb–Sr whole-rock isochron ages of 1370 ± 25 Ma, (2) type B or G_2 granitoids with an average age of 1308 ± 25 Ma, (3) type C or G_3 granitoids which were emplaced at around 1094 ± 50 Ma and (4) type D or G_4 tin-bearing granites yielding ages of 977 ± 18 Ma. Kampunzu et al. (1986), based on structural and petrofabric data, suggested that G_1, G_2 and G_3 Kibaran granitoids defined by Cahen et al. (1984) were part of a same igneous event. Tack et al. (2002) found only two bimodal magmatic episodes in the Kibaran Belt cropping out in Burundi based on SHRIMP single-zircon U–Pb, the first extensive synorogenic magmatism at 1370 Ma and a second post-orogenic magmatism at 1205 Ma. According to Tack et al. (2002) the first magmatic event includes all G_1, G_2 and G_3 granites defined by Cahen et al. (1984) and dated in Burundi between 1330 and 1185 Ma (Rb–Sr ages, Fernandez-Alonso et al., 1986; Klerkx et al., 1987) as suggested by Kampunzu et al. (1986). The 1205 Ma magmatic event is characterised by small bodies of shear-controlled A-type post-orogenic granitoids that were accompagnied by mafic intrusives. In this part of the Kibarn Belt, different pegamtites including Nb–Ta pegmatites were emplaced around 970 Ma.

In Mitwaba area, Kokonyangi et al. (2004, 2006, 2007) defined two deformational events, at 1.38 Ga (D1) and 1.08 Ga (D2) based on SHRIMP U–Pb zircon ages. Kokonyangi et al. (2006) tentatively found three magmatic cycles within the Kibaran Belt. The first cycle comprises mantle-derived arc-type mafic and closely related intermediate igneous bodies intruded between 1.4 and 1.38 Ga. The second magmatic event that includes intrusive bodies and lavas, post-dates D1 but is pre- or syn-D2. The third cycle is late-to post-D2 and includes tin–granites and related aplite, greisen and pegmatite bodies that were emplaced between 1.0 and 0.95 Ga.

The Irumide Belt in Zambia consists of a Paleoproterozoic to Mesoproterozoic complex of gneiss and granites, and supracrustal quartzites and pelites (De Waele and Mapani, 2002; De Waele et al., 2006a,b). Granitoid magmatism in the Irumide Belt occurred in two different intervals, between 1660–1550 Ma (Lukamfwa phase) and 1050–950 Ma (Irumide phase). These granitoids have highly negative $\varepsilon_{Nd}(t)$ values indicative of derivation from recycling of continental crust (De Waele et al., 2003, 2006a). In the Southern Irumide Belt,

low Th/U zircon rims and metamorphic monazite were dated at ∼1050 Ma, coeval with the magmatic phases between 1080 and 1030 Ma, indicating that both (arc) magmatism and peak metamorphism in the Southern Irumide Belt predates that in the Irumide Belt itself by ∼30 million years (Johnson et al., 2005, 2006).

In the Choma-Kalomo Block two generations of batholiths are known; the older was emplaced between 1352 and 1343 Ma and the younger between 1285 ± 64 and 1198 ± 6 Ma (Hanson et al., 1988; Johnson et al., 2005). Bulambo et al. (2004) found also similar ages for the two major magmatic events within the Choma-Kalomo Block dated by SHRIMP U–Pb on zircon at 1368 ± 10 Ma and ∼1180 Ma, respectively. These ages correspond to the two magmatic events defined by Tack et al. (2002) in the northern part of the Kibaran Belt (Burundi) dated at 1345 Ma and 1200 Ma. Based on whole-rock Sm/Nd isotope data on granites from the older generation (ca. 1350 Ma), Hanson et al. (1988) stated that the granitic magma, which interacted with sialic crust during the ascent, was not derived from an Archean source.

2.4. Neoproterozoic Katangan (Lufilian) Belt

Cahen et al. (1984) recognised three different compressional events in the evolution of the Katangan Belt. The older Lomamian orogeny occurred at ca. 950 Ma, the Lusaka folding around 840 Ma and a younger event named the Lufilian orogeny between 656 and 503 Ma. Kampunzu and Cailteux (1999) did not find any tectonic event older than 900 Ma in the evolution of the Katangan Belt. They described three different deformational phases in the Katangan Belt. The first event (Kolwezian or D1), occurred between ca. 800 and 710 Ma, the second (Monwezi or D2) between ca. 690 and 540 Ma and the third (Chilatembo or D3), which postdates the deposition of the Biano Subgroup (Ku 3, Table 1), is younger than 540 Ma.

The depositional history of the Katangan sedimentary rocks started with continental rifting related to the dispersal of the Rodinia Supercontinent ca. 880 Ma ago (Porada and Berhorst, 2000). According to Kampunzu et al. (2000), this rifting led to the formation of a young oceanic crust and was accompanied by magmatism witnessed by the Kafue rhyolite, the Nchanga granite and the Lusaka granite dated, respectively, at 879 Ma (Hanson et al., 1994), 877 Ma (Porada and Berhorst, 2000) and 865 Ma (Barr et al., 1977). This could correspond to the Lusaka folding event described by Cahen et al. (1984). John et al. (2004) and Rainaud et al. (2005) found age ranges of peak metamorphic events in the Lufilian around 532–529 Ma (U–Pb monazite) and 592–512 Ma (U–Pb monazite), which also include the collision age. These metamorphic ages correspond to the assembly of Gondwana at ca. 530 Ma (John et al., 2004).

3. Methodology

Heavy-mineral concentrate samples were collected from the sand of two small streams cross-cutting the Gungwania (sample JBM4, location: S10°24.729′–E27°57.027′) and Talala (sample JBM5, location: S10°16′28.4″–E27°56′34.7″) kimberlite pipes in the Kundelungu Plateau (Figs. 1 and 2). Heavy-mineral separation was carried out by the CSIRO Exploration and Mining Laboratory, North Ryde (Australia). Among the kimberlite indicator minerals (garnet, olivine, pyroxene, ilmenite, chromite, perovskite) separated from the concentrates, zircon grains were picked out individually, mounted in epoxy blocks and polished for analysis. The freshness of these minerals indicates that the sampling was done close to or inside the pipe. Two hundred and twenty-nine zircon grains were analysed. External form and internal structure were imaged using combined cathodoluminescence/BSE techniques in a Camebax SX100 electron microprobe (EMP) at GEMOC. Hf, Y, U, Th and Zr (oxide) contents were also analysed on the same EMP, using a range of natural and synthetic standards.

3.1. U–Pb dating

U–Pb dating of zircon used a Agilent 7500S ICP-MS attached to a Merchantek 213 nm New Wave Nd:YAG laser microprobe at GEMOC. The frequency for the analyses was 5 Hz, and the spot size for the laser was 30–50 μm. Belousova et al. (2001) and Jackson et al. (2004) have described in detail the analytical procedures used here.

The acquisition of signals is recorded as a function of time (ablation depth). The analysis takes approximately 3 min consisting of ∼60 s of background measurement followed by ablation. Data are acquired on five isotopes (^{206}Pb, ^{207}Pb, ^{208}Pb, ^{232}Th and ^{238}U) using the instrument's time-resolved-analysis data acquisition software. Mass discrimination in the mass spectrometer and residual elemental fractionation are corrected by calibration against a homogeneous standard zircon (GEMOC GJ-1, age 609 Ma). The analysis is performed in 'runs' of 16 analyses that include 12 unknowns bracketed at the beginning and the end by 2 analyses of the GJ-1 zircon standard. The "unknowns" include two near-concordant reference zircons, 91,500 (Wiedenbeck et al., 1995) and

le 1
thetised Lithostratigraphy of the Neoproterozoic Katangan Supergroup (François, 1973; Cailteux et al., 1994; Batumike et al., 2007)

ergroup	Group	Subgroup	Formation	Former nomenclature (François, 1987)	Members and lithologies
angan					
±500 Ma		Biano Ku 3			Arkoses, conglomerates, argillaceous sandstones
			Sampwe—Ku 2.3	Ks2.2	Dolomitic pelites, argillaceous to sandy siltstones
		Ku 2	Kiubo—Ku 2.2	Ks2.1	Dolomitic sandstones, siltstones and pelites
	Kundelungu Ku (formerly Upper Kundelungu)		Mongwe—Ku 2.1	Ks1.3	Dolomitic pelites, siltstones and sandstones
			Lubudi Ku 1.4	Ks 1.2.4	Alternating pink oolitic limestone (“calcaire de Lubudi”) and sar carbonate beds
		Gombela Ku 1 (formerly Likasi)	Kanianga—Ku 1.3	Ks 1.2.2 & 1.2.3	Carbonate siltstones and shales
			Lusele-Ku 1.2	Ks 1.2.1	Pink to grey micritic dolomite (Calcaire Rose)
			Kiandamu—Ku 1.1	Ks1.1	Petit Conglomerat tillite/diamictite
±620 Ma		Ng2	Monwezi—Ng 2.2	Ki 2	Dolomitic sandstones, siltstones and pelites
	Nguba Ng (formerly Upper Kundelungu)		Katete-Ng2.1	Ki 1.3	Dolomitic sandstones or siltstones in northern facies (formerly 1.3) to the north; alternating shale and dolomite beds (“Serie Rec rente”) to the south
			Kakontwe—Ng 1.3	Ki 1.2.2	Carbonates
		Muombe Ng1	Kaponda—Ng 1.2	Ki 1.2.1	Carbonate shales and siltstones; Dolomie Tigree at the base
			Mwale-Ng1.1	Ki 1.1	Grand Conglomerat tillite/diamictite
±750 Ma		Mwashya (formerly Upper Mwashya) R4	Kanzadi—R 4.3	Upper Mwashya R4.2	Sandstones or alternating siltstones and shales
			Kafubu—R 4.2		Carbonaceous shales
			Kamoya—R 4.1		Dolomitic shales, siltstones, sandstones, including conglomera beds and cherts in variable position
				Lower Mwashya R4.1	Kansuki—R 3.3.2: dolomites including volcaniclastic beds
	Roan R	Dipeta R3	R3.3		Mofya—R 3.3.1: dolomites, arenitic dolomites, dolomitic siltsto
			R 3.2		Argillaceous to dolomitic siltstones with interbedded feldspat sandstones or white dolomites; intrusive gabbros
			R3.1		Argillaceous dolomitic siltstones (R.G.S., “Roches Gre Schisteuses”)
		Mines R2	Kambove—R 2.3		Stromatolitic, laminated, shaly or talcose dolomites; locally sa stones at base; beds of siltstones at top
			Shales Dolomitiques R 2.2		Dolomitic shales including three carbonaceous horizons; occasio dolomites
			Kamoto—R 2.1		Stromatolitic dolomite (R.S.C.), silicified/arenitic dolomi (R.S.F./D.Strat), grey argillaceous dolomitic siltstone at the b (Grey R.A.T.)
		R.A.T. R1			Red argillaceous dolomitic siltstones and sandstones (“Roc Argilo-Talqueuses”)
±900 Ma	Base of the R.A.T. sequence unknown				Basal conglomerate

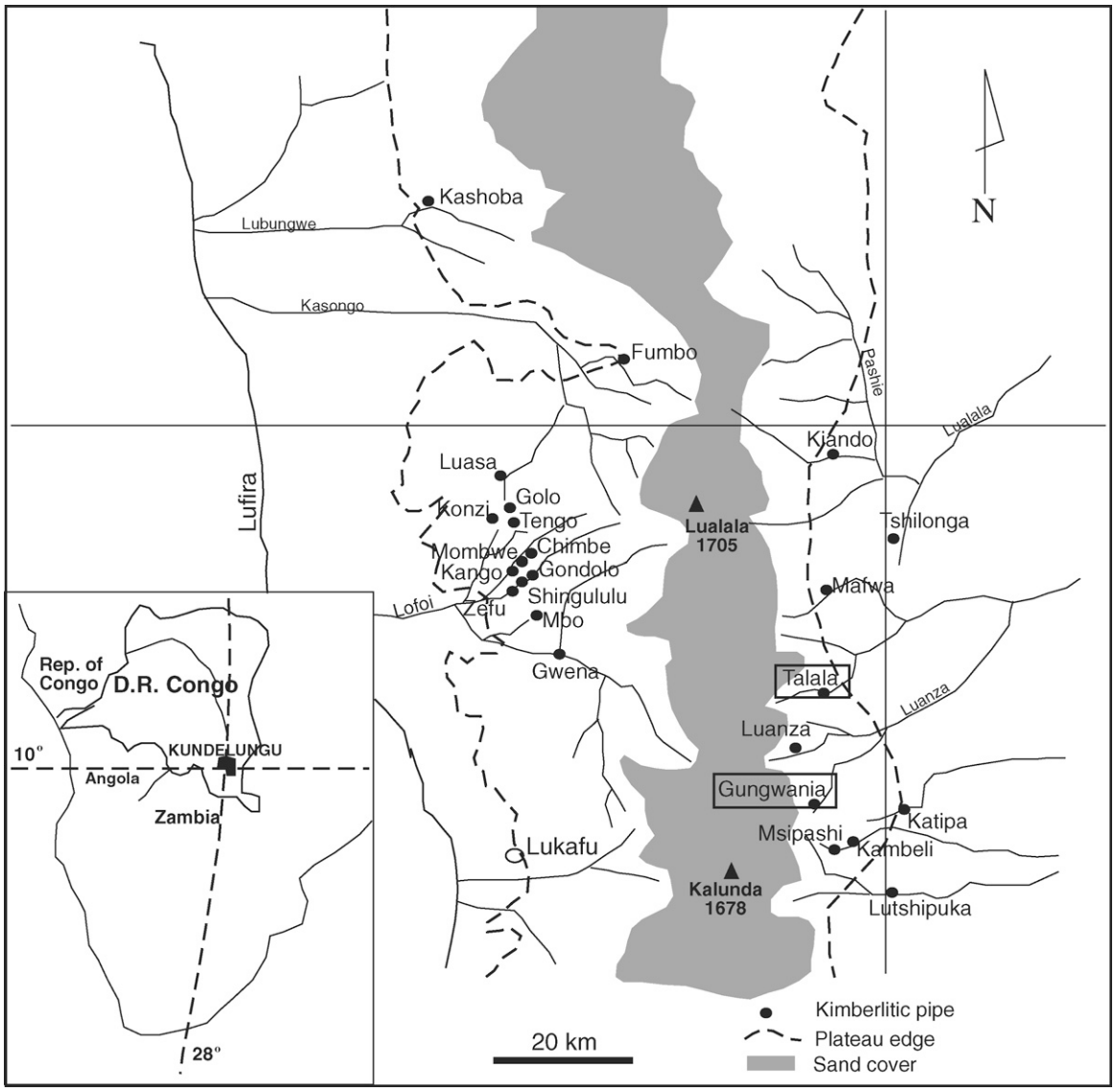

Fig. 2. Sample location (names in squares) within the Kundelungu Plateau (modified after Kampata, 1993).

Mud Tank (Black and Gulson, 1978), which are analysed before the samples and are used as independent control on reproducibility and instrument stability. The precision of the laser ablation ICPMS (LA-ICPMS) technique is discussed in detail by Jackson et al. (2004).

Isotope ratios are calculated from background-subtracted signals for the corresponding isotopes. Uncertainties in these ratios combine the uncertainties of signal and background, arising from counting statistics, added in quadrature. The same error propagation is used for both standards and unknowns. The standard ratios are interpolated between measurements of the unknowns. This procedure allows the propagation of uncertainties in the standard ratio measurements to estimate the standard ratio uncertainties relevant to each unknown ratio measurement. These relative uncertainties are then combined with those of the unknowns in quadrature. Furthermore, a 1% uncertainty (1σ) is assigned to the standard isotope ratios and is propagated through the error analysis. This procedure assures that the analytical uncertainties presented here are conservative (maximum probable) estimates.

U–Pb ages were calculated from raw signals using GLITTER (www.es.mq.edu.au/GEMOC; Van Achterbergh et al., 2001) version 4.4. This software permits the calculation of relevant isotopic ratios for

each mass sweep, and allows the isotopically homogeneous portion of the signal to be selected for integration. The calibration of each selected sample time-segment against the identical time-segments of the standard zircon (GJ) analyses allows the correction of integrated ratios for ablation-related fractionation and instrumental mass bias.

We applied the method of Andersen (2002) for common-lead correction on discordant analyses. This correction assumes that the observed $^{206}Pb/^{238}U$, $^{207}Pb/^{235}U$ and $^{208}Pb/^{232}Th$ ratios of a discordant zircon reflect a combination of common lead and lead loss at a defined time, and solves the resulting mass-balance equation. No correction was applied to analyses that are concordant within 2σ analytical errors in $^{206}Pb/^{238}U$ and $^{207}Pb/^{235}U$. Thirty-five analyses were corrected for common lead and 25 analyses that remained discordant were rejected for discussion in this study. The ages shown in the figures are $^{207}Pb/^{206}Pb$ ages for grains older than 1.0 Ga and $^{206}Pb/^{238}U$ ages for younger grains.

3.2. Hf-isotope determination

The Hf-isotope analyses presented here were performed in situ using a 213 nm Nd:YAG laser microprobe attached to a Nu Plasma multi-collector ICPMS system. Griffin et al. (2000, 2004) have described the methodology in detail. The analysis was carried out with a beam diameter of ~40 μm, a 5 Hz repetition rate, 60% power output and a laser energy of ~0.13 mJ. The ablation times were 100–200 s.

The chondritic values of Blichert-Toft et al. (1997) were used for the calculation of ε_{Hf} values. To calculate model ages (T_{DM}) based on a depleted-mantle source, a model with $(^{176}Hf/^{177}Hf)_I = 0.279718$ and $^{176}Hf/^{177}Hf = 0.0384$ was adopted. This provides a value of $^{176}Hf/^{177}Hf$ (0.28325) similar to that of average mid-ocean ridge basalt over 4.56 Ga. The T_{DM} ages that are calculated using measured $^{176}Lu/^{177}Hf$ of the zircon give thus the minimum age for the source material of the magma from which the zircon crystallised. A "crustal" model age (T^{C}_{DM}) was also calculated for each zircon grain; this calculation assumes that the parental magma was derived from the average continental crust ($^{176}Lu/^{177}Hf = 0.015$), which in turn was originally derived from the depleted mantle.

4. Results

229 zircon grains were analysed for morphology and structure, trace elements, U–Pb age and Hf-isotope composition. These results are presented in Table 2 and Figs. 4 and 5. The morphology of the analysed grains ranges from rounded to euhedral and internal structures may be diffuse, oscillatory, laminated or unzoned (Fig. 3; Table 2).

4.1. U–Pb data

Four main age populations were found in the analysed zircons; Archean, Paleoproterozoic, Mesoproterozoic and Neoproterozoic. These four groups correlate well with the main geological events previously described in the region. Most of the grains are concordant or near concordant, but the Neoarchean and Paleoproterozoic groups contain more discordant grains. One grain yields a Mesoarchean age (~3.3 Ga, sample JBM5-085, Table 2). Another grain gives an age of 2962 ± 18 Ma and there is a relatively large population at the end of late Archean time, centred on 2633 ± 15 Ma (Fig. 5). The zircon yielding a Mesoarchean age is well-rounded and without any internal structure. The late Archean zircons are mostly rounded, but there are a few euhedral grains. They show oscillatory or diffuse structures, or lack internal zonation.

Paleoproterozoic grains have ages spreading from 2.1 to 1.7 Ga (Fig. 5). A major peak occurs at 1882 ± 10 Ma, with minor ones at 2149 ± 11 Ma and 1788 ± 20 Ma. The grains are mostly euhedral, with few rounded forms, and most display oscillatory or diffuse structures, but some do not show any zoning (Fig. 4).

Mesoproterozoic zircons are euhedral to rounded; very few show oscillatory zonation, some have diffuse structure and some do not present zoning. A large population straddles the Mesoproterozoic–Neoproterozoic boundary at 1039 ± 26 Ma, and other peaks occur at 1557 ± 16, 1469 ± 11, 1339 ± 15 and 1192 ± 22 Ma. Neoproterozoic zircons show five different age peaks (Fig. 5). A large population is observed at 620 ± 17 Ma, followed in order of importance by peaks at 817 ± 10, 700 ± 7, 669 ± 7 and 568 ± 15 Ma. These grains are generally euhedral, though a few are rounded, and they show a combination of laminated or diffuse structures, or no zoning; very few have oscillatory structures.

4.2. Zircon source rocks

Trace-element compositions of zircon can provide broad information on the rock type that hosted the zircon (Belousova et al., 2002; Griffin et al., 2004). The methodology uses the Classification and Regression Tree (CART) software, applied to a large database of zircons from known rock types. It produces a classification tree (Fig. 6) that defines a zircon's source rock based on

Table 2
Analytical zircon data (for morphology 1: euhedral to 5: rounded)

Sample	EMP (wt%)			MC-ICPMS		LAM-ICPMS		Ratios							
	ZrO_2	HfO_2	Y_2O_3	Yb (ppm)	Lu (ppm)	Th (ppm)	U (ppm)	$^{207}Pb/^{206}Pb$	$\pm1\sigma$	$^{207}Pb/^{235}U$	$\pm1\sigma$	$^{206}Pb/^{238}U$	$\pm1\sigma$	$^{208}Pb/^{232}Th$	$\pm1\sigma$
JBM4-001	66.24	1.24	0.15	700	102	172	130	0.0801	0.0012	1.844	0.026	0.1667	0.0017	0.0291	0.0004
JBM4-002	66.18	1.13	0.05	263	54	33	62	0.0737	0.0009	1.760	0.019	0.1733	0.0014	0.0546	0.0006
JBM4-003	64.77	1.22	0.08	506	78	29	17	0.1113	0.0023	4.857	0.091	0.3166	0.0037	0.0910	0.0014
JBM4-004	65.56	1.72	0.16	528	76	149	552	0.0703	0.0008	1.597	0.015	0.1646	0.0014	0.0534	0.0006
JBM4-005	65.85	1.43	0.20	388	55	97	353	0.0609	0.0008	0.836	0.009	0.0995	0.0008	0.0314	0.0004
JBM4-006	66.78	1.49	0.08	407	67	39	73	0.1732	0.0018	11.904	0.099	0.4985	0.0040	0.1367	0.0013
JBM4-007	66.20	1.25	0.14	495	63	106	541	0.0594	0.0006	0.836	0.007	0.1021	0.0008	0.0328	0.0003
JBM4-008	66.38	1.20	0.32	785	109	173	729	0.0613	0.0006	0.949	0.008	0.1121	0.0009	0.0356	0.0003
JBM4-009	66.74	1.08	0.15	549	71	81	92	0.0969	0.0012	4.019	0.048	0.2996	0.0031	0.0915	0.0012
JBM4-010	65.36	1.55	0.25	2096	205	153	465	0.0739	0.0010	1.761	0.022	0.1732	0.0018	0.0540	0.0008
JBM4-011	66.09	1.00	0.17	465	68	197	157	0.0598	0.0008	0.754	0.009	0.0915	0.0008	0.0297	0.0003
JBM4-013	65.20	1.42	0.36	722	115	138	463	0.0627	0.0007	0.992	0.009	0.1148	0.0010	0.0356	0.0004
JBM4-013C	65.20	1.42	0.36	722	115	64	294	0.0628	0.0016	1.024	0.023	0.1183	0.0013	0.0363	0.0004
JBM4-015	66.49	1.51	0.01	461	84	128	95	0.1181	0.0015	5.425	0.062	0.3334	0.0033	0.1025	0.0011
JBM4-016	67.00	0.89	0.11	341	57	59	151	0.0727	0.0012	1.714	0.025	0.1710	0.0014	0.0517	0.0004
JBM4-017	65.74	1.17	0.26	504	85	279	229	0.1150	0.0012	5.287	0.044	0.3335	0.0027	0.0995	0.0008
JBM4-019	64.75	1.50	0.34	739	108	195	472	0.0657	0.0012	1.094	0.018	0.1207	0.0009	0.0369	0.0003
JBM4-021	65.84	1.38	0.01	341	61	212	181	0.0805	0.0012	1.984	0.027	0.1788	0.0018	0.0589	0.0007
JBM4-023	67.31	0.76	0.06	99	15	37	213	0.0607	0.0012	0.867	0.015	0.1037	0.0010	0.0320	0.0003
JBM4-024	65.55	1.06	0.03	138	21	19	100	0.0631	0.0012	1.016	0.017	0.1168	0.0010	0.0359	0.0003
JBM4-025	64.84	1.47	0.19	389	57	928	1780	0.0556	0.0068	0.260	0.031	0.0338	0.0005	0.0105	0.0003
JBM4-027	65.66	1.81	0.06	849	122	82	117	0.0727	0.0010	1.675	0.020	0.1671	0.0016	0.0521	0.0006
JBM4-028	64.57	1.94	0.50	4554	523	430	1269	0.0741	0.0008	1.841	0.021	0.1803	0.0019	0.0595	0.0007
JBM4-029	55.76	0.93	3.16	264	37	121	278	0.0710	0.0008	1.487	0.015	0.1520	0.0013	0.0487	0.0005
JBM4-030	66.08	1.41	0.12	520	77	197	349	0.0717	0.0014	1.650	0.030	0.1670	0.0015	0.0505	0.0004
JBM4-031	66.60	0.95	0.10	217	35	20	31	0.1126	0.0015	5.100	0.061	0.3287	0.0031	0.0977	0.0013
JBM4-032	66.41	1.55	0.04	683	99	99	160	0.1738	0.0021	11.850	0.137	0.4949	0.0052	0.1510	0.0021
JBM4-032C	66.41	1.55	0.04	683	99	408	330	0.1741	0.0039	9.744	0.183	0.4059	0.0049	0.1122	0.0013
JBM4-033	65.06	1.20	0.27	444	70	127	401	0.1090	0.0036	4.884	0.148	0.3250	0.0039	0.0941	0.0010
JBM4-034	65.16	1.56	0.18	501	69	532	854	0.0642	0.0012	0.861	0.016	0.0974	0.0012	0.0348	0.0008
JBM4-035	66.00	1.38	0.01	434	56	551	630	0.0907	0.0031	1.120	0.035	0.0896	0.0012	0.0264	0.0003
JBM4-036	65.65	1.52	0.24	1118	144	532	854	0.0720	0.0009	1.656	0.019	0.1669	0.0017	0.0535	0.0006
JBM4-037	64.57	1.05	0.38	209	29	282	936	0.0631	0.0009	0.987	0.013	0.1134	0.0010	0.0367	0.0004
JBM4-038	65.07	1.10	0.26	775	98	64	254	0.0671	0.0013	1.362	0.026	0.1474	0.0017	0.0461	0.0006
JBM4-039	65.45	1.37	0.12	517	75	247	330	0.1140	0.0015	5.232	0.063	0.3328	0.0032	0.0953	0.0009
JBM4-040	66.61	1.28	0.09	464	58	193	177	0.0618	0.0010	0.924	0.014	0.1085	0.0009	0.0345	0.0004
JBM4-041	65.90	1.28	0.10	30	4	57	114	0.1136	0.0013	5.129	0.052	0.3276	0.0031	0.0936	0.0008
JBM4-042	63.35	1.33	0.44	461	66	225	333	0.0698	0.0011	1.549	0.025	0.1610	0.0018	0.0490	0.0007
JBM4-043	65.32	1.50	0.20	1172	134	209	518	0.0619	0.0009	0.973	0.013	0.1140	0.0011	0.0358	0.0004
JBM4-044	65.37	1.41	0.17	1052	160	256	453	0.1765	0.0038	12.335	0.258	0.5066	0.0083	0.1400	0.0034
JBM4-045	65.50	1.42	0.11	351	48	54	118	0.0620	0.0010	0.974	0.015	0.1139	0.0011	0.0364	0.0006
JBM4-046	64.98	1.32	0.12	525	77	246	452	0.1128	0.0013	4.627	0.053	0.2976	0.0032	0.0803	0.0010
JBM4-047	65.25	1.49	0.10	451	68	246	115	0.1205	0.0013	5.733	0.052	0.3450	0.0029	0.0989	0.0008
JBM4-048	65.82	1.26	0.21	663	107	498	383	0.1147	0.0012	5.249	0.051	0.3318	0.0031	0.0968	0.0009
JBM4-050	65.34	1.32	0.27	347	51	184	139	0.1188	0.0014	5.698	0.061	0.3480	0.0034	0.1010	0.0010
JBM4-051	65.60	1.25	0.12	326	48	87	375	0.0610	0.0011	0.846	0.013	0.1006	0.0009	0.0310	0.0003
JBM4-052	64.77	1.16	0.37	946	127	152	411	0.0606	0.0007	0.843	0.008	0.1009	0.0009	0.0319	0.0003
JBM4-053	65.19	1.26	0.14	230	37	64	84	0.1831	0.0019	12.931	0.112	0.5123	0.0043	0.1382	0.0012
JBM4-054	65.29	1.30	0.07	506	80	262	256	0.1097	0.0031	4.773	0.123	0.3155	0.0037	0.0913	0.0010
JBM4-055	64.57	1.38	0.04	535	85	74	81	0.1165	0.0014	5.439	0.060	0.3385	0.0033	0.1001	0.0011
JBM4-056	64.61	1.34	0.41	671	100	185	689	0.0628	0.0009	0.939	0.013	0.1085	0.0012	0.0342	0.0006
JBM4-057	65.18	1.02	0.20	417	68	98	93	0.1167	0.0021	5.174	0.091	0.3215	0.0041	0.0836	0.0016
JBM4-058	64.16	1.68	0.17	435	71	135	228	0.0729	0.0008	1.693	0.016	0.1684	0.0015	0.0517	0.0005
JBM4-059	65.61	1.46	0.11	381	66	99	79	0.1196	0.0013	5.835	0.051	0.3538	0.0028	0.1042	0.0009
JBM4-060	64.82	1.18	0.14	522	87	100	112	0.1167	0.0013	5.410	0.049	0.3363	0.0028	0.0983	0.0008
JBM4-061	66.09	1.62	0.16	415	60	159	263	0.0666	0.0008	1.247	0.014	0.1358	0.0012	0.0419	0.0004
JBM4-062	57.58	1.13	3.66	1650	171	2570	2477	0.0679	0.0035	0.298	0.015	0.0318	0.0004	0.0097	0.0001
JBM4-063	65.87	1.36	0.03	289	45	35	36	0.0730	0.0017	1.634	0.037	0.1623	0.0019	0.0505	0.0009
JBM4-064	65.88	1.16	0.08	628	77	58	252	0.0610	0.0010	0.791	0.013	0.0941	0.0010	0.0297	0.0006
JBM4-066	65.89	1.43	0.12	389	57	73	166	0.0735	0.0014	1.685	0.031	0.1662	0.0018	0.0508	0.0007
JBM4-067	65.80	1.22	0.28	341	46	41	119	0.0743	0.0017	1.756	0.039	0.1714	0.0019	0.0546	0.0010
JBM4-069	63.76	1.53	0.68	1350	168	305	551	0.0798	0.0009	2.053	0.023	0.1866	0.0018	0.0509	0.0005
JBM4-070	64.75	1.68	0.28	598	97	135	299	0.0595	0.0017	0.812	0.021	0.0989	0.0010	0.0306	0.0003
JBM4-071	65.20	1.75	0.05	774	122	234	193	0.1147	0.0017	5.331	0.077	0.3371	0.0037	0.0932	0.0010
JBM4-072	65.36	1.31	0.10	579	91	60	110	0.0612	0.0019	0.905	0.027	0.1073	0.0013	0.0337	0.0006
JBM4-073	65.26	1.42	0.16	413	61	123	113	0.0770	0.0029	1.726	0.063	0.1626	0.0024	0.0301	0.0007
JBM4-074	65.61	1.34	0.12	260	37	96	216	0.0739	0.0009	1.746	0.018	0.1712	0.0014	0.0534	0.0005
JBM4-075	65.24	1.06	0.11	1102	125	258	450	0.0665	0.0013	1.215	0.025	0.1326	0.0016	0.0414	0.0006
JBM4-077	64.45	1.21	0.45	1000	145	352	281	0.0743	0.0015	1.767	0.035	0.1726	0.0020	0.0523	0.0006
JBM4-078	61.72	1.10	0.27	953	131	259	304	0.0615	0.0012	0.850	0.016	0.1004	0.0012	0.0312	0.0005
JBM4-080	65.44	1.06	0.31	1412	201	267	210	0.1211	0.0016	1.744	0.021	0.1045	0.0011	0.0292	0.0003

Table 2 (*Continued*)

Sample	EMP (wt%)			MC-ICPMS		LAM-ICPMS		Ratios							
	ZrO_2	HfO_2	Y_2O_3	Yb (ppm)	Lu (ppm)	Th (ppm)	U (ppm)	$^{207}Pb/^{206}Pb$	±1σ	$^{207}Pb/^{235}U$	±1σ	$^{206}Pb/^{238}U$	±1σ	$^{208}Pb/^{232}Th$	±1σ
JBM4-082	65.15	1.49	0.11	565	73	267	210	0.0729	0.0024	0.964	0.030	0.0960	0.0015	0.0140	0.0005
JBM4-083	64.99	1.51	0.24	501	67	198	224	0.0727	0.0010	1.689	0.023	0.1686	0.0018	0.0524	0.0007
JBM4-084	64.82	1.20	0.11	369	54	149	243	0.1128	0.0018	5.138	0.079	0.3304	0.0040	0.1043	0.0016
JBM4-086	65.54	1.47	0.26	1559	204	121	112	0.0738	0.0009	1.758	0.021	0.1728	0.0017	0.0538	0.0007
JBM4-087	65.86	0.98	0.18	514	69	155	366	0.0751	0.0013	1.696	0.027	0.1639	0.0017	0.0509	0.0008
JBM4-088	65.11	1.63	0.07	236	34	87	130	0.1164	0.0017	5.542	0.077	0.3454	0.0039	0.1028	0.0015
JBM4-089	65.62	1.25	0.13	470	70	75	84	0.1150	0.0015	5.022	0.067	0.3168	0.0036	0.0738	0.0010
JBM4-090C	65.68	1.10	0.17	698	92	440	201	0.0741	0.0009	1.759	0.022	0.1722	0.0018	0.0533	0.0007
JBM4-090r	65.68	1.10	0.17	698	92	28	112	0.0817	0.0013	2.219	0.033	0.1969	0.0022	0.0515	0.0012
JBM4-092	65.38	1.33	0.16	786	125	96	115	0.0743	0.0009	1.801	0.017	0.1759	0.0013	0.0545	0.0005
JBM4-093	65.06	1.51	0.09	352	57	60	75	0.1712	0.0028	11.434	0.155	0.4843	0.0045	0.1341	0.0012
JBM4-094	65.24	1.62	0.13	633	98	90	214	0.0607	0.0008	0.845	0.010	0.1010	0.0009	0.0326	0.0004
JBM4-095	65.05	1.48	0.16	346	61	184	314	0.1093	0.0012	4.280	0.045	0.2839	0.0028	0.0833	0.0008
JBM4-096	64.77	1.20	0.02	103	18	83	260	0.0595	0.0010	0.800	0.013	0.0976	0.0011	0.0296	0.0005
JBM4-097	65.36	1.03	0.15	180	30	17	23	0.0793	0.0013	1.949	0.029	0.1782	0.0017	0.0614	0.0008
JBM4-098	65.59	1.16	0.17	452	65	59	136	0.0733	0.0010	1.757	0.022	0.1738	0.0017	0.0535	0.0007
JBM4-099	64.89	1.48	0.15	493	75	770	520	0.1278	0.0016	4.818	0.064	0.2731	0.0032	0.0705	0.0009
JBM4-100	65.34	1.37	0.28	696	92	202	393	0.0749	0.0008	1.805	0.019	0.1748	0.0016	0.0550	0.0005
JBM4-101	65.12	1.18	0.01	148	23	355	469	0.0671	0.0010	0.828	0.010	0.0894	0.0008	0.0313	0.0003
JBM4-102	65.45	1.68	0.05	607	76	184	338	0.1794	0.0020	10.611	0.121	0.4290	0.0047	0.0680	0.0009
JBM4-103	63.85	1.28	0.27	500	91	129	203	0.0704	0.0016	1.542	0.033	0.1589	0.0014	0.0482	0.0004
JBM4-104	64.96	1.67	0.07	850	121	116	284	0.0724	0.0013	1.659	0.028	0.1662	0.0019	0.0535	0.0010
JBM4-105	64.83	1.93	0.25	310	49	54	97	0.0598	0.0009	0.758	0.010	0.0919	0.0008	0.0299	0.0004
JBM4-106	65.06	1.36	0.02	260	50	151	100	0.1178	0.0014	5.545	0.059	0.3413	0.0032	0.1012	0.0009
JBM4-107	66.22	1.38	0.07	183	29	44	87	0.1190	0.0014	5.598	0.054	0.3411	0.0028	0.1002	0.0012
JBM4-108	60.81	1.31	1.22	582	73	680	1616	0.1798	0.0033	7.621	0.113	0.3074	0.0033	0.0847	0.0011
JBM4-109	64.09	1.55	0.12	528	71	663	887	0.1356	0.0032	2.320	0.049	0.1241	0.0014	0.0351	0.0004
JBM4-110	65.11	1.45	0.21	448	62	241	501	0.1238	0.0013	6.163	0.058	0.3611	0.0033	0.1069	0.0009
JBM4-111	65.69	1.40	0.18	843	119	97	583	0.0669	0.0010	0.851	0.012	0.0923	0.0010	0.0239	0.0005
JBM4-112	65.25	1.42	0.32	447	58	118	245	0.0612	0.0007	0.842	0.009	0.0997	0.0009	0.0314	0.0003
JBM4-112r	65.25	1.42	0.32	447	58	213	757	0.0609	0.0006	0.861	0.008	0.1026	0.0008	0.0326	0.0003
JBM4-113	65.33	1.15	0.23	236	34	38	75	0.0611	0.0023	0.922	0.032	0.1093	0.0016	0.0349	0.0012
JBM4-114	64.94	1.37	0.16	484	66	97	240	0.1996	0.0021	15.464	0.151	0.5620	0.0053	0.1505	0.0015
JBM4-115	65.06	1.30	0.18	738	101	283	175	0.1154	0.0013	5.504	0.062	0.3458	0.0035	0.1029	0.0010
JBM4-116	63.27	1.63	0.58	1962	223	802	1545	0.0908	0.0026	0.847	0.023	0.0677	0.0007	0.0200	0.0003
JBM4-117	65.70	1.22	0.16	563	84	213	226	0.1161	0.0013	5.240	0.049	0.3274	0.0028	0.0959	0.0008
JBM4-118	65.71	1.21	0.17	641	99	9	31	0.0747	0.0014	1.779	0.030	0.1727	0.0017	0.0539	0.0013
JBM4-119	65.68	1.31	0.06	419	59	297	540	0.0744	0.0019	1.729	0.039	0.1685	0.0019	0.0508	0.0005
JBM4-120	65.15	1.27	0.11	266	38	93	521	0.0642	0.0008	1.047	0.013	0.1183	0.0012	0.0366	0.0006
JBM4-121	63.23	1.23	1.03	1292	187	652	757	0.0859	0.0013	1.515	0.023	0.1279	0.0015	0.0322	0.0005
JBM4-122	65.33	1.38	0.07	262	37	209	625	0.0635	0.0007	1.015	0.011	0.1159	0.0011	0.0368	0.0004
JBM4-123	65.48	1.36	0.16	345	51	204	1029	0.0632	0.0007	0.999	0.011	0.1148	0.0012	0.0370	0.0004
JBM4-124	65.43	0.92	0.51	1158	159	84	177	0.0736	0.0011	1.725	0.026	0.1701	0.0019	0.0544	0.0009
JBM4-125	65.35	1.51	0.05	986	142	41	334	0.0662	0.0012	1.047	0.016	0.1148	0.0010	0.0350	0.0003
JBM4-127	64.90	1.06	0.07	350	54	356	365	0.0600	0.0008	0.825	0.011	0.0997	0.0010	0.0321	0.0003
JBM4-128	66.01	1.39	0.20	930	153	443	277	0.1177	0.0015	4.620	0.051	0.2846	0.0027	0.0778	0.0008
JBM4-129	64.96	1.56	0.07	631	106	286	282	0.1140	0.0015	5.309	0.075	0.3378	0.0041	0.1061	0.0015
JBM4-131	65.09	1.14	0.43	552	89	84	80	0.0737	0.0015	1.751	0.034	0.1726	0.0019	0.0542	0.0009
JBM4-132	66.40	1.15	0.12	544	92	145	133	0.1142	0.0014	5.227	0.063	0.3320	0.0035	0.1024	0.0011
JBM4-134	65.26	1.41	0.09	561	106	23	67	0.0761	0.0018	1.965	0.044	0.1873	0.0025	0.0569	0.0017
JBM4-135	64.70	1.48	0.47	1239	187	157	457	0.0728	0.0009	1.723	0.020	0.1717	0.0017	0.0548	0.0007
JBM4-136	64.92	1.48	0.48	630	93	128	359	0.0665	0.0008	1.239	0.012	0.1352	0.0011	0.0413	0.0004
JBM4-137	65.65	1.62	0.15	514	83	152	440	0.0744	0.0009	1.796	0.019	0.1751	0.0017	0.0542	0.0006
JBM4-138	66.11	1.17	0.15	564	82	150	138	0.1220	0.0014	5.866	0.055	0.3486	0.0029	0.0900	0.0008
JBM4-139	65.02	1.42	0.07	275	40	81	107	0.0750	0.0017	1.807	0.038	0.1748	0.0023	0.0550	0.0011
JBM4-140	63.58	1.41	0.41	576	83	190	1109	0.1129	0.0012	5.195	0.050	0.3338	0.0031	0.0962	0.0009
JBM4-141	65.51	1.45	0.13	517	83	175	248	0.1148	0.0013	5.207	0.059	0.3289	0.0035	0.0943	0.0010
JBM4-142	65.28	1.48	0.05	891	113	163	150	0.1143	0.0012	5.079	0.046	0.3223	0.0028	0.0948	0.0008
JBM4-143	65.10	1.51	0.06	797	126	286	436	0.1906	0.0032	13.797	0.183	0.5249	0.0053	0.1438	0.0014
JBM4-144	65.30	1.06	0.20	876	128	35	49	0.0758	0.0012	1.802	0.027	0.1725	0.0018	0.0565	0.0008
JBM4-145	65.47	1.28	0.12	283	41	30	53	0.0633	0.0013	0.934	0.018	0.1070	0.0012	0.0347	0.0006
JBM4-146	64.64	1.45	0.10	409	58	107	169	0.0689	0.0008	1.285	0.014	0.1353	0.0013	0.0450	0.0005
JBM4-147	62.63	1.69	0.54	643	92	72	*111*	0.0686	0.0014	1.431	0.025	0.1514	0.0015	0.0461	0.0004
JBM4-148	65.81	1.27	0.18	611	76	205	209	0.1804	0.0040	12.135	0.226	0.4878	0.0058	0.1344	0.0015
JBM4-149	65.24	1.29	0.15	522	71	136	209	0.0719	0.0008	1.662	0.016	0.1677	0.0015	0.0542	0.0005
JBM4-150	66.32	1.30	0.06	153	21	20	16	0.1736	0.0038	11.825	0.230	0.4942	0.0051	0.1366	0.0013
JBM4-151	65.59	1.58	0.12	556	88	52	122	0.0624	0.0008	0.955	0.011	0.1110	0.0010	0.0359	0.0004
JBM4-152	65.29	1.29	0.17	1033	131	189	527	0.0655	0.0007	1.175	0.010	0.1301	0.0011	0.0389	0.0004
JBM4-153	66.07	1.07	0.13	407	62	215	209	0.1181	0.0015	5.722	0.076	0.3516	0.0041	0.1030	0.0013
JBM4-154	65.25	1.45	0.39	710	99	63	105	0.0723	0.0017	1.704	0.036	0.1710	0.0016	0.0517	0.0004
JBM4-155	64.78	1.16	0.36	401	60	625	360	0.1151	0.0012	5.232	0.053	0.3299	0.0032	0.0955	0.0009
JBM4-156	65.07	1.36	0.18	646	87	127	439	0.0629	0.0010	1.005	0.016	0.1160	0.0014	0.0356	0.0007

Table 2 (*Continued*)

Sample	EMP (wt%)			MC-ICPMS		LAM-ICPMS		Ratios							
	ZrO_2	HfO_2	Y_2O_3	Yb (ppm)	Lu (ppm)	Th (ppm)	U (ppm)	$^{207}Pb/^{206}Pb$	$\pm1\sigma$	$^{207}Pb/^{235}U$	$\pm1\sigma$	$^{206}Pb/^{238}U$	$\pm1\sigma$	$^{208}Pb/^{232}Th$	$\pm1\sigma$
JBM4-157	64.81	1.49	0.08	331	53	181	169	0.1151	0.0015	5.254	0.071	0.3313	0.0039	0.0987	0.0013
JBM4-159r	64.22	1.27	0.36	1052	119	142	474	0.0608	0.0009	0.845	0.011	0.1009	0.0010	0.0337	0.0005
JBM4-160	64.80	1.82	0.05	597	55	43	304	0.0740	0.0012	1.831	0.030	0.1795	0.0022	0.0548	0.0016
JBM4-162	65.23	1.16	0.17	1213	153	144	156	0.0740	0.0011	1.726	0.024	0.1692	0.0018	0.0537	0.0007
JBM4-163	65.69	1.39	0.05	975	164	102	102	0.1154	0.0013	5.399	0.051	0.3393	0.0030	0.0975	0.0009
JBM4-164	64.28	1.13	0.58	767	122	370	247	0.0753	0.0011	1.842	0.027	0.1775	0.0020	0.0549	0.0007
JBM4-165	64.19	1.12	0.19	764	122	164	260	0.0620	0.0011	0.798	0.014	0.0933	0.0011	0.0321	0.0005
JBM4-166	63.17	1.16	1.08	4061	490	4545	1517	0.1937	0.0021	2.730	0.030	0.1023	0.0011	0.0286	0.0003
JBM4-167	65.29	1.48	0.09	709	107	169	239	0.0727	0.0013	1.528	0.027	0.1526	0.0018	0.0502	0.0008
JBM4-168	66.30	1.17	0.41	726	109	379	591	0.1879	0.0020	13.057	0.152	0.5043	0.0056	0.1385	0.0016
JBM4-169	64.73	1.22	0.14	818	130	459	257	0.1156	0.0013	5.675	0.052	0.3561	0.0029	0.1089	0.0009
JBM4-170	65.00	1.21	0.40	582	92	279	176	0.1161	0.0012	5.428	0.051	0.3393	0.0030	0.1012	0.0009
JBM4-170r	65.00	1.21	0.40	582	92	234	171	0.1160	0.0013	5.374	0.054	0.3359	0.0031	0.0988	0.0009
JBM4-171	64.89	1.41	0.15	406	69	107	192	0.0745	0.0008	1.764	0.017	0.1718	0.0015	0.0539	0.0005
JBM4-172	64.93	1.10	0.00	204	35	136	309	0.0952	0.0019	3.357	0.066	0.2560	0.0036	0.0771	0.0022
JBM4-173	65.39	1.31	0.07	502	84	100	59	0.1143	0.0015	5.362	0.069	0.3404	0.0036	0.0993	0.0011
JBM4-174	65.51	1.16	0.16	328	51	14	46	0.0741	0.0012	1.731	0.024	0.1695	0.0015	0.0512	0.0010
JBM4-175	65.72	1.84	0.00	91	12	186	367	0.0701	0.0010	1.369	0.018	0.1417	0.0013	0.0425	0.0006
JBM4-176	64.62	1.38	0.03	352	60	63	58	0.0730	0.0010	1.711	0.022	0.1700	0.0015	0.0517	0.0005
JBM4-177	64.66	1.14	0.22	735	119	576	316	0.1130	0.0014	5.194	0.065	0.3335	0.0038	0.1008	0.0011
JBM4-177r	64.66	1.14	0.22	735	119	329	209	0.1149	0.0012	5.195	0.050	0.3280	0.0030	0.0967	0.0009
JBM4-178	65.39	1.27	0.03	1166	124	94	178	0.1772	0.0021	12.233	0.136	0.5006	0.0051	0.1467	0.0021
JBM4-179	65.62	1.23	0.31	338	57	184	152	0.1167	0.0017	5.472	0.071	0.3400	0.0035	0.1008	0.0013
JBM4-180	64.40	1.37	0.15	587	85	294	400	0.0922	0.0012	2.006	0.023	0.1579	0.0016	0.0598	0.0007
JBM4-181	64.83	1.26	0.07	233	37	107	138	0.0589	0.0014	0.754	0.018	0.0930	0.0012	0.0293	0.0006
JBM4-182	64.88	1.04	0.12	475	72	17	47	0.0723	0.0018	1.684	0.038	0.1689	0.0017	0.0511	0.0005
JBM4-183	63.80	1.26	1.07	2423	393	70	159	0.0739	0.0017	1.731	0.038	0.1700	0.0022	0.0548	0.0014
JBM4-184	63.71	1.26	0.52	1345	161	168	856	0.1343	0.0014	5.420	0.045	0.2928	0.0023	0.0849	0.0009
JBM4-185	64.80	1.09	0.24	221	29	52	173	0.0586	0.0010	0.836	0.013	0.1036	0.0011	0.0328	0.0006
JBM4-186	65.48	1.50	0.15	713	106	230	268	0.1083	0.0024	4.733	0.093	0.3170	0.0032	0.0918	0.0009
JBM4-188	65.77	1.10	0.21	386	57	111	89	0.1154	0.0013	5.237	0.053	0.3293	0.0031	0.0955	0.0009
JBM4-189	65.61	0.95	0.38	346	50	17	79	0.0621	0.0019	0.900	0.027	0.1051	0.0015	0.0354	0.0016
JBM4-190	65.25	1.22	0.07	532	72	106	168	0.0741	0.0014	1.750	0.031	0.1714	0.0020	0.0547	0.0010
JBM4-191	65.36	1.03	0.12	199	29	9	22	0.0615	0.0020	0.899	0.028	0.1060	0.0012	0.0352	0.0009
JBM4-192	65.10	1.30	0.26	634	93	137	147	0.0720	0.0015	1.631	0.033	0.1644	0.0021	0.0501	0.0009
JBM4-195	65.33	1.39	0.06	336	49	110	127	0.1779	0.0020	12.299	0.140	0.5016	0.0054	0.1362	0.0015
JBM4-195r	65.33	1.39	0.06	336	49	139	230	0.1655	0.0024	10.593	0.138	0.4644	0.0050	0.1336	0.0025
JBM4-196	65.22	1.10	0.13	299	45	228	160	0.1756	0.0020	11.949	0.135	0.4936	0.0052	0.1384	0.0015
JBM4-198	65.10	1.38	0.17	3728	510	162	563	0.1320	0.0015	6.283	0.079	0.3453	0.0040	0.0968	0.0014
JBM4-200	64.92	1.29	0.10	202	31	71	136	0.0749	0.0015	1.753	0.034	0.1698	0.0022	0.0529	0.0011
JBM4-201	64.27	1.42	0.27	1113	156	228	529	0.1176	0.0013	5.357	0.058	0.3304	0.0034	0.0947	0.0011
JBM4-202	65.11	1.26	0.11	251	37	41	96	0.0742	0.0015	1.691	0.030	0.1653	0.0017	0.0492	0.0011
JBM4-203	65.42	1.30	0.17	450	69	163	93	0.0709	0.0009	1.604	0.019	0.1642	0.0015	0.0496	0.0005
JBM4-204	64.95	1.02	0.28	513	79	89	110	0.0622	0.0016	0.977	0.024	0.1139	0.0015	0.0356	0.0007
JBM4-205	66.03	1.44	0.01	30	4	39	83	0.0624	0.0011	0.940	0.014	0.1093	0.0009	0.0345	0.0006
JBM4-206	65.85	1.11	0.01	263	46	24	60	0.0721	0.0012	1.620	0.023	0.1630	0.0015	0.0494	0.0009
JBM4-207	65.32	1.45	0.13	342	52	64	182	0.0605	0.0011	0.861	0.016	0.1033	0.0012	0.0319	0.0007
JBM4-208	66.45	1.30	0.11	326	54	61	124	0.0733	0.0012	1.782	0.027	0.1764	0.0017	0.0540	0.0009
JBM4-209	65.69	1.06	0.10	581	93	56	104	0.0654	0.0020	1.194	0.034	0.1324	0.0019	0.0425	0.0013
JBM4-210	65.30	1.55	0.11	284	48	370	480	0.0738	0.0009	1.876	0.024	0.1843	0.0020	0.0590	0.0007
JBM4-211	64.80	1.61	0.23	613	97	220	426	0.0651	0.0009	1.188	0.016	0.1324	0.0014	0.0404	0.0005
JBM4-212	65.35	1.43	0.08	283	45	107	241	0.0609	0.0008	0.849	0.010	0.1012	0.0009	0.0317	0.0004
JBM4-214	65.57	1.47	0.08	128	22	225	262	0.1185	0.0012	5.676	0.051	0.3476	0.0030	0.1021	0.0009
JBM4-215	65.16	1.56	0.36	406	67	61	176	0.0733	0.0014	1.725	0.032	0.1708	0.0020	0.0544	0.0013
JBM4-216	64.37	1.93	0.05	242	42	61	124	0.0741	0.0010	1.764	0.020	0.1727	0.0014	0.0526	0.0006
JBM4-216r	64.37	1.93	0.05	242	42	312	1163	0.0760	0.0009	1.886	0.022	0.1800	0.0019	0.0536	0.0007
JBM4-217	64.18	1.73	0.20	672	103	138	546	0.0726	0.0009	1.614	0.019	0.1613	0.0016	0.0502	0.0007
JBM4-218	64.88	1.11	0.05	263	42	105	140	0.0668	0.0020	1.153	0.033	0.1255	0.0019	0.0416	0.0011
JBM4-219	64.07	1.13	0.67	1101	151	244	521	0.0639	0.0017	1.076	0.025	0.1223	0.0013	0.0375	0.0004
JBM4-219r	64.07	1.13	0.67	1101	151	101	286	0.0639	0.0009	1.025	0.013	0.1164	0.0011	0.0348	0.0005
JBM4-220	64.24	1.01	0.57	938	142	515	665	0.0785	0.0030	1.555	0.056	0.1436	0.0019	0.0430	0.0005
JBM4-221	63.98	1.20	0.31	528	92	226	223	0.1158	0.0015	5.365	0.065	0.3361	0.0035	0.0997	0.0012
JBM4-222	64.66	0.98	0.19	578	103	164	165	0.1157	0.0015	5.459	0.067	0.3423	0.0036	0.0816	0.0010
JBM4-223	63.54	1.14	0.64	603	91	105	245	0.0733	0.0009	1.748	0.020	0.1730	0.0016	0.0525	0.0006
JBM4-224	65.05	1.11	0.32	639	103	221	229	0.0732	0.0009	1.586	0.017	0.1571	0.0014	0.0475	0.0005
JBM4-226	64.14	0.93	1.09	582	92	47	84	0.0682	0.0016	1.273	0.028	0.1354	0.0016	0.0431	0.0010
JBM4-227	65.40	1.78	0.14	177	25	115	312	0.0617	0.0008	0.930	0.011	0.1093	0.0010	0.0346	0.0004
JBM4-227C	65.40	1.78	0.14	177	25	46	56	0.0624	0.0011	0.954	0.016	0.1108	0.0011	0.0357	0.0008
JBM4-228	65.91	1.09	0.20	663	114	45	181	0.0723	0.0013	1.639	0.028	0.1644	0.0017	0.0537	0.0008
JBM4-229	65.30	1.19	0.26	787	127	218	161	0.1098	0.0013	4.823	0.044	0.3188	0.0025	0.0901	0.0008
JBM4-230	65.08	1.19	0.27	431	68	155	171	0.0748	0.0010	1.814	0.021	0.1759	0.0017	0.0539	0.0006
JBM5-001	64.73	1.23	0.08	421	54	7	328	0.1337	0.0015	6.308	0.072	0.34226	0.0036	0.09171	0.0016

Table 2 (*Continued*)

Sample	EMP (wt%)			MC-ICPMS		LAM-ICPMS		Ratios							
	ZrO_2	HfO_2	Y_2O_3	Yb (ppm)	Lu (ppm)	Th (ppm)	U (ppm)	$^{207}Pb/^{206}Pb$	±1σ	$^{207}Pb/^{235}U$	±1σ	$^{206}Pb/^{238}U$	±1σ	$^{208}Pb/^{232}Th$	±1σ
JBM5-003	64.11	1.58	0.65	1338	165	11	92	0.1179	0.0014	5.341	0.060	0.32843	0.00316	0.08482	0.0018
JBM5-005	65.20	1.27	0.34	1077	131	205	599	0.1151	0.0015	5.169	0.064	0.32562	0.00333	0.09193	0.0022
JBM5-006	64.71	1.37	0.33	1563	166	181	476	0.1218	0.0013	1.810	0.019	0.10783	0.00105	0.02041	0.0003
JBM5-007	64.30	1.38	0.19	827	98	10	86	0.1177	0.0013	5.241	0.057	0.32301	0.00321	0.09006	0.0016
JBM5-013	65.62	1.39	0.16	855	100	167	313	0.1159	0.0013	5.291	0.054	0.33114	0.00317	0.09601	0.0016
JBM5-015	64.46	1.35	0.09	375	42	285	927	0.1259	0.0014	6.428	0.067	0.37038	0.00359	0.10637	0.0018
JBM5-016	65.17	1.13	0.16	608	66	96	243	0.1149	0.0013	5.506	0.060	0.34746	0.00341	0.10315	0.0019
JBM5-022	66.46	0.87	0.13	619	67	28	448	0.1149	0.0013	5.244	0.055	0.33104	0.00322	0.09582	0.0015
JBM5-029	66.04	1.20	0.20	740	81	25	195	0.1140	0.0013	5.297	0.058	0.33694	0.00345	0.09535	0.0017
JBM5-034	64.80	1.59	0.20	2233	233	15	263	0.1143	0.0012	5.444	0.055	0.34545	0.00336	0.09677	0.0015
JBM5-039	66.30	1.41	0.13	700	81	316	1895	0.1139	0.0013	5.228	0.059	0.33305	0.00341	0.09617	0.0018
JBM5-040	64.86	1.42	0.34	1007	122	7	272	0.1139	0.0012	5.229	0.052	0.33297	0.00328	0.09794	0.0013
JBM5-043	66.23	1.37	0.25	856	100	10	76	0.1147	0.0012	5.273	0.054	0.33349	0.00329	0.0987	0.0014
JBM5-049	23.31	0.01	0.06	8	1	11	72	0.1149	0.0013	5.291	0.056	0.33404	0.00328	0.09429	0.0016
JBM5-052	65.64	1.41	0.03	572	66	84	180	0.1127	0.0020	4.983	0.090	0.32063	0.00416	0.09243	0.0038
JBM5-056	65.40	1.21	0.04	244	27	3	28	0.1805	0.0020	11.694	0.117	0.46983	0.0044	0.12428	0.0019
JBM5-058	64.57	1.41	0.23	934	102	1	22	0.1149	0.0015	5.279	0.072	0.33337	0.00389	0.0969	0.0024
JBM5-060	65.43	1.24	0.09	242	28	2	73	0.1214	0.0013	5.796	0.060	0.34618	0.00341	0.09971	0.0015
JBM5-085	65.60	1.30	0.17	541	67	99	46	0.2683	0.0029	24.215	0.252	0.65453	0.00646	0.18085	0.003
JBM5-103	65.09	1.22	0.21	464	51	20	112	0.1259	0.0013	6.503	0.069	0.37473	0.00383	0.11149	0.0017
JBM5-121	65.24	1.76	0.11	1380	160	22	271	0.2175	0.0024	17.443	0.183	0.58171	0.00565	0.14998	0.0027
JBM5-125	65.98	1.58	0.10	383	45	30	102	0.1784	0.0020	12.032	0.129	0.4893	0.00489	0.14097	0.0025
JBM5-157	64.51	1.54	0.13	647	82	34	97	0.1810	0.0019	11.902	0.124	0.47693	0.00484	0.11116	0.0016
JBM5-181	65.96	1.50	0.16	4091	348	8	42	0.1713	0.0030	10.419	0.188	0.44117	0.00575	0.08582	0.0035

Sample	Ages (Ma)						
	$^{207}Pb/^{206}U$	±1σ	$^{207}Pb/^{235}U$	±1σ	$^{206}Pb/^{238}U$	±1σ	$^{208}Pb/^{232}Th$
JBM4-001	1200	13	1061	9	994	10	580
JBM4-002	1032	10	1031		1030	8	1075
JBM4-003	1820	18	1795	16	1773	18	1760
JBM4-004	937	9	969	6	982	8	1051
JBM4-005	636	12	617	5	611	5	625
JBM4-006	2589	6	2597	8	2607	17	2590
JBM4-007	580	9	617	4	627	5	652
JBM4-008	651	8	677	4	685	5	708
JBM4-009	1566	10	1638	10	1689	15	1769
JBM4-010	1038	12	1031	8	1030	10	1063
JBM4-011	596	13	571	5	564	5	591
JBM4-013	696	9	700	5	701	6	707
JBM4-013C	700	54	716	11	721	7	722
JBM4-015	1927	9	1889	10	1855	16	1973
JBM4-016	1005	35	1014	10	1018	8	1018
JBM4-017	1880	7	1867	7	1855	13	1918
JBM4-019	797	38	750	9	735	5	732
JBM4-021	1209	13	1110	9	1061	10	1158
JBM4-023	628	43	634	8	636	6	636
JBM4-024	712	41	712	8	712	6	712
JBM4-025	438	277	234	25	214	3	212
JBM4-027	1005	11	999	8	996	9	1027
JBM4-028	1045	10	1060	7	1069	10	1168
JBM4-029	956	9	925	6	912	7	962
JBM4-030	976	42	989	11	995	8	997
JBM4-031	1841	10	1836	10	1832	15	1885
JBM4-032	2594	9	2593	11	2592	23	2843
JBM4-032C	2597	38	2411	17	2196	23	2149
JBM4-033	1783	61	1799	26	1814	19	1817
JBM4-034	749	20	631	9	599	7	691
JBM4-035	1440	66	763	17	553	7	527
JBM4-036	985	11	992	7	995	9	1052
JBM4-037	712	13	697	7	693	6	728
JBM4-038	839	21	873	11	886	9	911
JBM4-039	1864	10	1858	10	1852	15	1840
JBM4-040	665	17	664	7	664	5	685
JBM4-041	1857	8	1841	9	1827	15	1809
JBM4-042	921	16	950	10	963	10	966
JBM4-043	671	13	690	7	696	6	711
JBM4-044	2621	16	2630	20	2642	36	2648
JBM4-045	674	17	690	8	695	6	722
JBM4-046	1845	9	1754	10	1680	16	1562
JBM4-047	1964	7	1936	8	1911	14	1906
JBM4-048	1876	8	1861	8	1847	15	1867

Table 2 (*Continued*)

Sample	Ages (Ma)						
	$^{207}Pb/^{206}U$	$\pm1\sigma$	$^{207}Pb/^{235}U$	$\pm1\sigma$	$^{206}Pb/^{238}U$	$\pm1\sigma$	$^{208}Pb/^{232}Th$
JBM4-050	1938	9	1931	9	1925	16	1945
JBM4-051	639	39	623	7	618	5	618
JBM4-052	626	9	621	4	619	5	634
JBM4-053	2681	6	2675	8	2666	18	2616
JBM4-054	1795	53	1780	22	1768	18	1765
JBM4-055	1904	9	1891	9	1880	16	1928
JBM4-056	700	14	672	7	664	7	680
JBM4-057	1907	15	1848	15	1797	20	1624
JBM4-058	1012	9	1006	6	1003	8	1018
JBM4-059	1951	7	1952	8	1953	13	2003
JBM4-060	1906	7	1887	8	1869	14	1896
JBM4-061	825	11	822	6	821	7	830
JBM4-062	866	111	264	12	202	2	195
JBM4-063	1015	27	983	14	969	11	996
JBM4-064	638	18	592	7	580	6	591
JBM4-066	1029	21	1003	12	991	10	1001
JBM4-067	1051	27	1030	14	1020	10	1075
JBM4-069	1193	10	1133	8	1103	10	1004
JBM4-070	587	62	603	12	608	6	608
JBM4-071	1875	12	1874	12	1873	18	1802
JBM4-072	646	43	654	14	657	7	670
JBM4-073	1121	49	1018	23	971	13	600
JBM4-074	1040	9	1026	7	1019	8	1051
JBM4-075	822	23	808	11	803	9	820
JBM4-077	1049	22	1033	13	1026	11	1030
JBM4-078	656	21	625	9	616	7	622
JBM4-080	1972	10	1025	8	641	6	582
JBM4-082	1010	38	685	16	591	9	281
JBM4-083	1004	13	1004	9	1005	10	1032
JBM4-084	1845	13	1842	13	1840	19	2006
JBM4-086	1037	11	1030	8	1027	10	1059
JBM4-087	1071	16	1007	10	978	9	1003
JBM4-088	1902	11	1907	12	1912	18	1977
JBM4-089	1880	11	1823	11	1774	18	1439
JBM4-090C	1044	11	1030	8	1024	10	1049
JBM4-090r	1239	14	1187	11	1159	12	1014
JBM4-092	1049	8	1046	6	1045	7	1072
JBM4-093	2570	28	2559	13	2546	20	2543
JBM4-094	627	12	622	5	621	5	648
JBM4-095	1788	9	1690	9	1611	14	1617
JBM4-096	586	17	597	7	600	6	589
JBM4-097	1181	15	1098	10	1057	9	1204
JBM4-098	1023	12	1030	8	1033	9	1054
JBM4-099	2068	10	1788	11	1557	16	1377
JBM4-100	1066	9	1047	7	1038	9	1082
JBM4-101	842	13	612	6	552	5	623
JBM4-102	2647	8	2490	11	2301	21	1329
JBM4-103	939	48	947	13	951	8	951
JBM4-104	998	17	993	11	991	11	1054
JBM4-105	596	16	573	6	567	5	595
JBM4-106	1923	8	1908	9	1893	15	1948
JBM4-107	1942	8	1916	8	1892	13	1930
JBM4-108	2651	31	2187	13	1728	16	1643
JBM4-109	2171	43	1218	15	754	8	698
JBM4-110	2012	8	1999	8	1987	15	2053
JBM4-111	834	14	625	7	569	6	477
JBM4-112	647	10	620	5	613	5	624
JBM4-112r	635	8	631	4	630	5	648
JBM4-113	644	50	663	17	669	10	693
JBM4-114	2823	7	2844	9	2875	22	2833
JBM4-115	1886	9	1901	10	1915	17	1979
JBM4-116	1442	57	623	13	422	4	400
JBM4-117	1897	7	1859	8	1826	14	1851
JBM4-118	1060	19	1038	11	1027	9	1061
JBM4-119	1053	51	1019	14	1004	10	1001
JBM4-120	748	12	727	6	721	7	727
JBM4-121	1337	14	936	9	776	9	640
JBM4-122	725	10	711	6	707	6	730
JBM4-123	714	10	703	6	700	7	734
JBM4-124	1029	15	1018	10	1013	10	1071
JBM4-125	812	38	727	8	700	6	696
JBM4-127	604	13	611	6	613	6	639
JBM4-128	1922	9	1753	9	1614	13	1515

Table 2 (*Continued*)

Sample	Ages (Ma)						
	$^{207}Pb/^{206}U$	$\pm1\sigma$	$^{207}Pb/^{235}U$	$\pm1\sigma$	$^{206}Pb/^{238}U$	$\pm1\sigma$	$^{208}Pb/^{232}Th$
JBM4-129	1864	11	1870	12	1876	20	2038
JBM4-131	1032	22	1028	12	1026	10	1067
JBM4-132	1867	10	1857	10	1848	17	1971
JBM4-134	1097	25	1104	15	1107	13	1119
JBM4-135	1008	11	1017	7	1022	10	1078
JBM4-136	821	9	818	5	818	6	818
JBM4-137	1053	10	1044	7	1040	9	1067
JBM4-138	1986	7	1956	8	1928	14	1741
JBM4-139	1069	23	1048	14	1038	12	1082
JBM4-140	1846	8	1852	8	1857	15	1857
JBM4-141	1877	9	1854	10	1833	17	1822
JBM4-142	1869	7	1833	8	1801	13	1831
JBM4-143	2748	28	2736	13	2720	22	2716
JBM4-144	1089	15	1046	10	1026	10	1110
JBM4-145	719	22	670	9	655	7	689
JBM4-146	896	10	839	6	818	7	890
JBM4-147	885	42	902	10	909	8	910
JBM4-148	2657	38	2615	17	2561	25	2548
JBM4-149	982	9	994	6	1000	8	1067
JBM4-150	2592	38	2591	18	2589	22	2588
JBM4-151	687	11	681	6	679	6	712
JBM4-152	790	8	789	5	788	6	772
JBM4-153	1927	11	1935	11	1942	20	1982
JBM4-154	995	49	1010	14	1017	9	1019
JBM4-155	1881	8	1858	9	1838	16	1844
JBM4-156	705	16	706	8	707	8	706
JBM4-157	1881	11	1861	12	1844	19	1902
JBM4-159r	632	14	622	6	619	6	670
JBM4-160	1042	16	1057	11	1064	12	1079
JBM4-162	1042	13	1018	9	1007	10	1057
JBM4-163	1886	8	1885	8	1883	14	1880
JBM4-164	1077	14	1061	10	1053	11	1081
JBM4-165	675	19	595	8	575	6	638
JBM4-166	2774	8	1337	8	628	6	570
JBM4-167	1005	18	942	11	916	10	990
JBM4-168	2724	9	2684	11	2632	24	2622
JBM4-169	1889	7	1928	8	1964	14	2090
JBM4-170	1896	8	1889	8	1883	14	1948
JBM4-170r	1896	8	1881	9	1867	15	1904
JBM4-171	1054	9	1032	6	1022	8	1062
JBM4-172	1532	18	1494	15	1469	19	1502
JBM4-173	1868	11	1879	11	1889	18	1913
JBM4-174	1043	15	1020	9	1010	8	1009
JBM4-175	932	13	876	8	854	8	841
JBM4-176	1013	12	1013	8	1012	8	1018
JBM4-177	1848	10	1852	11	1855	18	1941
JBM4-177r	1878	8	1852	8	1829	15	1866
JBM4-178	2627	8	2622	10	2617	22	2766
JBM4-179	1907	11	1896	11	1886	17	1941
JBM4-180	1471	10	1118	8	945	9	1174
JBM4-181	562	30	571	10	573	7	584
JBM4-182	994	52	1002	15	1006	9	1007
JBM4-183	1038	24	1020	14	1012	12	1078
JBM4-184	2155	6	1888	7	1655	11	1648
JBM4-185	551	18	617	7	635	6	653
JBM4-186	1771	41	1773	16	1775	16	1775
JBM4-188	1886	8	1859	9	1835	15	1843
JBM4-189	679	39	652	14	644	9	702
JBM4-190	1044	18	1027	11	1020	11	1076
JBM4-191	657	46	651	15	650	7	700
JBM4-192	986	22	982	13	981	12	988
JBM4-195	2633	8	2628	11	2621	23	2580
JBM4-195r	2512	10	2488	12	2459	22	2534
JBM4-196	2612	8	2600	11	2586	23	2619
JBM4-198	2125	10	2016	11	1912	19	1867
JBM4-200	1066	20	1028	13	1011	12	1041
JBM4-201	1920	9	1878	9	1841	16	1829
JBM4-202	1048	20	1005	12	986	9	970
JBM4-203	953	11	972	7	980	8	979
JBM4-204	681	31	692	12	695	9	708
JBM4-205	687	18	673	7	668	5	686
JBM4-206	988	16	978	9	973	8	975

Table 2 (*Continued*)

Sample	Ages (Ma)						
	$^{207}Pb/^{206}U$	$\pm1\sigma$	$^{207}Pb/^{235}U$	$\pm1\sigma$	$^{206}Pb/^{238}U$	$\pm1\sigma$	$^{208}Pb/^{232}Th$
JBM4-207	621	20	631	8	634	7	635
JBM4-208	1021	16	1039	10	1047	9	1063
JBM4-209	787	37	798	16	802	11	841
JBM4-210	1037	11	1073	8	1090	11	1158
JBM4-211	777	12	795	7	801	8	801
JBM4-212	635	12	624	6	621	5	630
JBM4-214	1933	7	1928	8	1923	14	1965
JBM4-215	1023	20	1018	12	1017	11	1071
JBM4-216	1044	11	1032	7	1027	8	1036
JBM4-216r	1095	11	1076	8	1067	10	1055
JBM4-217	1003	11	976	7	964	9	990
JBM4-218	830	35	779	15	762	11	824
JBM4-219	737	56	742	12	744	8	744
JBM4-219r	737	14	716	7	710	6	691
JBM4-220	1160	78	953	22	865	11	852
JBM4-221	1892	10	1879	10	1868	17	1921
JBM4-222	1891	10	1894	10	1898	17	1585
JBM4-223	1022	10	1026	7	1029	9	1035
JBM4-224	1020	10	965	7	941	8	938
JBM4-226	874	26	834	12	819	9	853
JBM4-227	663	12	668	6	669	6	687
JBM4-227C	689	19	680	8	677	7	710
JBM4-228	996	19	985	11	981	9	1056
JBM4-229	1795	7	1789	8	1784	12	1743
JBM4-230	1063	11	1050	8	1044	9	1061
JBM5-001	2147	20	2020	10	1898	17	1774
JBM5-003	1925	22	1875	10	1831	15	1646
JBM5-005	1882	24	1847	10	1817	16	1778
JBM5-006	1982	20	1049	7	660	6	408
JBM5-007	1921	21	1859	9	1804	16	1743
JBM5-013	1894	20	1867	9	1844	15	1853
JBM5-015	2041	20	2036	9	2031	17	2043
JBM5-016	1879	21	1901	9	1922	16	1984
JBM5-022	1878	20	1860	9	1843	16	1849
JBM5-029	1864	20	1868	9	1872	17	1841
JBM5-034	1869	20	1892	9	1913	16	1867
JBM5-039	1862	21	1857	10	1853	16	1856
JBM5-040	1863	19	1857	9	1853	16	1889
JBM5-043	1875	19	1865	9	1855	16	1903
JBM5-049	1878	20	1867	9	1858	16	1821
JBM5-052	1844	33	1816	15	1793	20	1787
JBM5-056	2658	18	2580	9	2483	19	2368
JBM5-058	1878	24	1865	12	1855	19	1869
JBM5-060	1977	20	1946	9	1916	16	1921
JBM5-085	3296	17	3277	10	3246	25	3360
JBM5-103	2041	19	2046	9	2052	18	2136
JBM5-121	2962	18	2960	10	2956	23	2825
JBM5-125	2638	19	2607	10	2568	21	2666
JBM5-157	2662	18	2597	10	2514	21	2130
JBM5-181	2570	30	2473	17	2356	26	1664

Sample	$\pm1\sigma$	Disc. (%)	Composition of Pb (%)	$^{176}Hf/^{177}Hf$	$\pm1\sigma$	$^{176}Lu/^{177}Hf$	$^{176}Yb/^{177}Hf$	T_{DM} (Ga)
JBM4-001	8	18.4	0.00	0.282365	0.000012	0.001350	0.045319	1.22
JBM4-002	11	0.2	0.00	0.282399	0.000008	0.000785	0.018750	1.16
JBM4-003	26	3	0.00	0.281551	0.000009	0.001051	0.033330	2.30
JBM4-004	11	−5.2	0.00	0.282093	0.000012	0.000723	0.024736	1.57
JBM4-005	8	4.1	0.00	0.282505	0.000008	0.000626	0.021830	1.01
JBM4-006	23	−0.8	0.00	0.281264	0.000010	0.000738	0.022001	2.66
JBM4-007	6	−8.5	0.00	0.282528	0.000008	0.000821	0.031879	0.99
JBM4-008	6	−5.5	0.00	0.282607	0.000007	0.001483	0.052431	0.89
JBM4-009	21	−9.4	0.00	0.281696	0.000009	0.001086	0.040962	2.11
JBM4-010	15	1.1	0.00	0.282205	0.000016	0.002176	0.109068	1.47
JBM4-011	5	5.6	0.00	0.282501	0.000009	0.001123	0.037466	1.03
JBM4-013	7	−0.7	0.00	0.282234	0.000009	0.001328	0.040969	1.40
JBM4-013C	8	−3.1	1.08	0.282234	0.000009	0.001328	0.040969	1.40
JBM4-015	20	4.3	0.00	0.281519	0.000011	0.000914	0.024636	2.34
JBM4-016	8	−1.3	0.24	0.282309	0.000009	0.001057	0.030819	1.29
JBM4-017	14	1.5	0.00	0.281523	0.000010	0.001193	0.034584	2.35
JBM4-019	5	8.3	0.35	0.282399	0.000007	0.001179	0.039527	1.17
JBM4-021	14	13.3	0.00	0.281845	0.000006	0.000733	0.019931	1.90
JBM4-023	6	−1.3	0.20	0.282510	0.000006	0.000321	0.010461	1.00
JBM4-024	6	−0.1	0.14	0.282510	0.000006	0.000321	0.010461	1.00

Table 2 (*Continued*)

Sample	±1σ	Disc. (%)	Composition of Pb (%)	$^{176}Hf/^{177}Hf$	±1σ	$^{176}Lu/^{177}Hf$	$^{176}Yb/^{177}Hf$	T_{DM} (Ga)
JBM4-025	7	51.9	22.01	0.282447	0.000007	0.000632	0.021254	1.09
JBM4-027	12	1	0.00	0.282017	0.000008	0.001104	0.037808	1.69
JBM4-028	14	−2.4	0.00	0.282374	0.000009	0.004419	0.188826	1.32
JBM4-029	10	5	0.00	0.282073	0.000005	0.000652	0.022893	1.59
JBM4-030	8	−2.2	0.37	0.282307	0.000008	0.000902	0.029677	1.29
JBM4-031	24	0.6	0.00	0.281661	0.000007	0.000594	0.018330	2.13
JBM4-032	37	0.2	0.00	0.281108	0.000007	0.001047	0.035510	2.89
JBM4-032C	24	18.2	1.11	0.281108	0.000007	0.001047	0.035510	2.89
JBM4-033	18	−2	1.81	0.281535	0.000008	0.000961	0.029748	2.32
JBM4-034	15	21.1	0.00	0.282488	0.000008	0.000720	0.025816	1.04
JBM4-035	6	64.2	2.10	0.282344	0.000007	0.000660	0.025240	1.23
JBM4-036	11	−1	0.00	0.282073	0.000009	0.001556	0.059365	1.63
JBM4-037	8	2.9	0.00	0.282469	0.000014	0.000453	0.016094	1.06
JBM4-038	11	−6	0.00	0.282392	0.000006	0.001473	0.056998	1.19
JBM4-039	17	0.8	0.00	0.281530	0.000009	0.000897	0.030287	2.32
JBM4-040	7	0.2	0.00	0.282215	0.000012	0.000746	0.029106	1.40
JBM4-041	16	1.9	0.00	0.282516	0.000005	0.000047	0.001895	0.98
JBM4-042	13	−4.8	0.00	0.282275	0.000007	0.000814	0.027981	1.33
JBM4-043	7	−3.9	0.18	0.282478	0.000008	0.001466	0.062771	1.07
JBM4-044	61	−1	0.00	0.280966	0.000012	0.001871	0.060148	3.14
JBM4-045	11	−3.2	0.00	0.282262	0.000009	0.000553	0.019905	1.34
JBM4-046	18	10.2	0.00	0.281383	0.000013	0.000954	0.031921	2.52
JBM4-047	15	3.2	0.02	0.281186	0.000006	0.000755	0.024431	2.77
JBM4-048	16	1.8	0.00	0.281504	0.000008	0.001391	0.042428	2.39
JBM4-050	18	0.8	0.00	0.281500	0.000033	0.000632	0.021214	2.35
JBM4-051	5	3.4	0.16	0.282535	0.000014	0.000627	0.020916	0.97
JBM4-052	6	1.1	0.00	0.282573	0.000012	0.001797	0.065605	0.95
JBM4-053	22	0.7	0.00	0.281094	0.000008	0.000481	0.014687	2.87
JBM4-054	18	1.7	0.76	0.281526	0.000007	0.001013	0.031294	2.34
JBM4-055	20	1.5	0.00	0.281526	0.000007	0.001013	0.031294	2.34
JBM4-056	11	5.4	0.12	0.282590	0.000007	0.001219	0.040223	0.91
JBM4-057	29	6.6	0.00	0.281611	0.000027	0.001098	0.033031	2.23
JBM4-058	9	0.9	0.00	0.281993	0.000010	0.000698	0.020891	1.70
JBM4-059	16	−0.1	0.00	0.281420	0.000005	0.000744	0.021013	2.46
JBM4-060	15	2.3	0.25	0.281463	0.000008	0.001205	0.035622	2.43
JBM4-061	9	0.6	0.00	0.282113	0.000007	0.000605	0.020664	1.54
JBM4-062	2	77.9	8.82	0.282307	0.000012	0.002475	0.117321	1.34
JBM4-063	17	4.8	0.00	0.281577	0.000013	0.000546	0.017129	2.24
JBM4-064	13	9.6	0.09	0.282534	0.000009	0.001091	0.043499	0.98
JBM4-066	14	3.9	0.08	0.281933	0.000009	0.000654	0.021989	1.78
JBM4-067	19	3.2	0.00	0.281780	0.000009	0.000622	0.022442	1.98
JBM4-069	9	8.2	0.00	0.281956	0.000008	0.001809	0.071157	1.80
JBM4-070	5	−3.7	0.21	0.282300	0.000008	0.000946	0.028663	1.30
JBM4-071	19	0.2	0.00	0.281566	0.000010	0.001143	0.035662	2.29
JBM4-072	12	−1.7	0.00	0.281566	0.000010	0.001143	0.035662	2.29
JBM4-073	14	14.4	0.00	0.282242	0.000007	0.000707	0.023472	1.37
JBM4-074	9	2.2	0.00	0.282018	0.000010	0.000458	0.015649	1.66
JBM4-075	11	2.5	0.00	0.282498	0.000008	0.001944	0.083983	1.06
JBM4-077	12	2.4	0.00	0.282289	0.000009	0.001967	0.066638	1.35
JBM4-078	10	6.3	0.14	0.282271	0.000014	0.001948	0.069504	1.37
JBM4-080	6	70.8	0.00	0.282183	0.000019	0.003097	0.106869	1.54
JBM4-082	11	43.4	0.00	0.282428	0.000009	0.000807	0.030579	1.12
JBM4-083	14	0.0	0.00	0.282306	0.000008	0.000729	0.026684	1.28
JBM4-084	30	0.3	0.00	0.281538	0.000007	0.000734	0.024683	2.30
JBM4-086	13	1	0.00	0.282096	0.000008	0.002272	0.085265	1.63
JBM4-087	15	9.4	0.33	0.282224	0.000009	0.001164	0.042262	1.41
JBM4-088	28	−0.6	0.00	0.281344	0.000010	0.000344	0.011669	2.53
JBM4-089	18	6.5	0.00	0.281563	0.000009	0.000925	0.030330	2.28
JBM4-090C	12	2	0.00	0.282291	0.000010	0.001379	0.051187	1.33
JBM4-090r	23	7.1	0.00	0.282291	0.000010	0.001379	0.051187	1.33
JBM4-092	9	0.4	0.00	0.282063	0.000009	0.001535	0.047519	1.64
JBM4-093	22	1.1	0.33	0.280926	0.000007	0.000616	0.018787	3.09
JBM4-094	7	1.1	0.00	0.282373	0.000008	0.000993	0.031533	1.20
JBM4-095	15	11.2	0.12	0.281533	0.000008	0.000677	0.018894	2.31
JBM4-096	11	−2.5	0.00	0.282509	0.000009	0.000248	0.006904	1.00
JBM4-097	15	11.3	0.00	0.281953	0.000011	0.000483	0.014114	1.74
JBM4-098	14	−1	0.00	0.281877	0.000008	0.000919	0.031384	1.86
JBM4-099	17	27.7	0.00	0.281455	0.000007	0.000835	0.026849	2.42
JBM4-100	10	2.9	0.00	0.282278	0.000009	0.001109	0.040937	1.33
JBM4-101	7	35.9	0.00	0.282494	0.000009	0.000314	0.010066	1.02
JBM4-102	17	15.5	0.00	0.281021	0.000006	0.000745	0.029162	2.98
JBM4-103	8	−1.3	0.51	0.282115	0.000014	0.001163	0.031366	1.56
JBM4-104	20	0.7	0.00	0.281916	0.000009	0.001184	0.040895	1.82
JBM4-105	7	5.2	0.00	0.282392	0.000006	0.000413	0.012913	1.16
JBM4-106	17	1.8	0.00	0.281478	0.000005	0.000601	0.015419	2.37

Table 2 (*Continued*)

Sample	±1σ	Disc. (%)	Composition of Pb (%)	$^{176}Hf/^{177}Hf$	±1σ	$^{176}Lu/^{177}Hf$	$^{176}Yb/^{177}Hf$	T_{DM} (Ga)
JBM4-107	21	3	0.18	0.281483	0.000007	0.000340	0.010710	2.35
JBM4-108	21	39.6	3.87	0.280948	0.000007	0.000912	0.035648	3.09
JBM4-109	8	69	4.48	0.281554	0.000012	0.000756	0.027404	2.28
JBM4-110	16	1.4	0.00	0.281418	0.000005	0.000708	0.024903	2.46
JBM4-111	11	33.1	0.00	0.282514	0.000006	0.001399	0.048416	1.02
JBM4-112	6	5.5	0.15	0.282451	0.000006	0.000670	0.025411	1.09
JBM4-112r	5	0.9	0.00	0.282451	0.000006	0.000670	0.025411	1.09
JBM4-113	24	−4.1	0.00	0.282344	0.000006	0.000480	0.016559	1.22
JBM4-114	25	−2.3	0.00	0.281010	0.000008	0.000793	0.028453	3.00
JBM4-115	18	−1.8	0.00	0.281621	0.000007	0.001274	0.045571	2.22
JBM4-116	5	73	5.53	0.282469	0.000008	0.002241	0.096881	1.11
JBM4-117	15	4.3	0.26	0.281640	0.000011	0.001125	0.037179	2.19
JBM4-118	24	3.4	0.16	0.282452	0.000008	0.001346	0.042547	1.10
JBM4-119	10	5.1	0.43	0.282053	0.000009	0.000742	0.025728	1.62
JBM4-120	12	3.9	0.03	0.282437	0.000010	0.000494	0.016859	1.10
JBM4-121	10	44.5	0.00	0.282316	0.000011	0.002490	0.084416	1.33
JBM4-122	8	2.7	0.00	0.282479	0.000007	0.000436	0.015232	1.04
JBM4-123	9	2	0.00	0.282577	0.000007	0.000617	0.020362	0.91
JBM4-124	17	1.8	0.00	0.282493	0.000018	0.002852	0.101818	1.09
JBM4-125	6	14.5	0.14	0.282533	0.000010	0.001538	0.052412	1.00
JBM4-127	7	−1.5	0.00	0.282487	0.000010	0.000837	0.026494	1.04
JBM4-128	15	18	0.00	0.281579	0.000008	0.001798	0.053737	2.31
JBM4-129	28	−0.7	0.00	0.281586	0.000008	0.001120	0.032669	2.26
JBM4-131	17	0.7	0.00	0.281997	0.000010	0.001274	0.038927	1.72
JBM4-132	21	1.2	0.00	0.281536	0.000011	0.001314	0.038054	2.34
JBM4-134	33	−0.9	0.00	0.282367	0.000007	0.001232	0.032030	1.22
JBM4-135	13	−1.5	0.00	0.282317	0.000007	0.002072	0.067324	1.31
JBM4-136	8	0.4	0.00	0.282319	0.000009	0.001033	0.034368	1.28
JBM4-137	11	1.3	0.00	0.282297	0.000005	0.000838	0.025587	1.30
JBM4-138	15	3.4	0.00	0.281644	0.000007	0.001152	0.038713	2.19
JBM4-139	21	3.1	0.00	0.281943	0.000008	0.000462	0.015549	1.75
JBM4-140	16	−0.6	0.00	0.281537	0.000009	0.000961	0.032884	2.32
JBM4-141	19	2.7	0.00	0.281530	0.000009	0.000943	0.028668	2.33
JBM4-142	15	4.2	0.37	0.281523	0.000010	0.001259	0.048559	2.35
JBM4-143	25	1.2	0.34	0.281078	0.000006	0.001370	0.042565	2.95
JBM4-144	15	6.3	0.00	0.281877	0.000008	0.001984	0.066561	1.92
JBM4-145	12	9.3	0.00	0.282295	0.000005	0.000523	0.017853	1.29
JBM4-146	9	9.3	0.00	0.282404	0.000013	0.000658	0.022778	1.15
JBM4-147	8	−2.9	0.34	0.282102	0.000011	0.000892	0.030626	1.56
JBM4-148	27	4.3	0.61	0.280093	0.000450	0.000978	0.038736	4.20
JBM4-149	10	−1.9	0.00	0.282211	0.000008	0.000904	0.032495	1.42
JBM4-150	24	0.2	0.87	0.281053	0.000010	0.000269	0.009491	2.90
JBM4-151	8	1.3	0.00	0.282564	0.000009	0.000915	0.028266	0.94
JBM4-152	7	0.2	0.00	0.282580	0.000009	0.001665	0.064464	0.94
JBM4-153	23	−0.9	0.00	0.281636	0.000011	0.000944	0.030516	2.19
JBM4-154	8	−2.5	0.38	0.282337	0.000007	0.001113	0.039285	1.25
JBM4-155	17	2.6	0.18	0.281501	0.000009	0.000840	0.027754	2.36
JBM4-156	13	−0.4	0.00	0.282635	0.000011	0.001049	0.038240	0.85
JBM4-157	23	2.3	0.00	0.281687	0.000010	0.000589	0.017956	2.10
JBM4-159r	10	2.1	0.00	0.282417	0.000009	0.001532	0.066522	1.16
JBM4-160	30	−2.3	0.00	0.281971	0.000008	0.000497	0.026427	1.72
JBM4-162	13	3.6	0.00	0.282087	0.000013	0.002167	0.084291	1.64
JBM4-163	16	0.2	0.00	0.281598	0.000011	0.001949	0.056666	2.30
JBM4-164	12	2.4	0.00	0.281753	0.000006	0.001780	0.054855	2.08
JBM4-165	10	15.5	0.00	0.281753	0.000006	0.001780	0.054855	2.08
JBM4-166	6	81	1.38	0.281654	0.000027	0.006941	0.282319	2.56
JBM4-167	16	9.6	0.00	0.282158	0.000011	0.001190	0.038518	1.50
JBM4-168	28	4.1	0.01	0.281123	0.000008	0.001518	0.049749	2.91
JBM4-169	17	−4.6	0.00	0.281497	0.000008	0.001752	0.054093	2.42
JBM4-170	16	0.8	0.00	0.281484	0.000011	0.001249	0.038687	2.41
JBM4-170r	17	1.8	0.00	0.281484	0.000011	0.001249	0.038687	2.41
JBM4-171	10	3.3	0.00	0.282271	0.000006	0.000801	0.023189	1.33
JBM4-172	40	4.7	0.18	0.281518	0.000009	0.000515	0.014899	2.32
JBM4-173	20	−1.3	0.00	0.281537	0.000007	0.001062	0.030964	2.32
JBM4-174	19	3.5	0.01	0.282335	0.000008	0.000715	0.022733	1.24
JBM4-175	12	9	0.00	0.282393	0.000006	0.000108	0.003996	1.15
JBM4-176	10	0.1	0.00	0.281994	0.000008	0.000721	0.020586	1.70
JBM4-177	21	−0.5	0.00	0.281562	0.000009	0.001713	0.051701	2.33
JBM4-177r	16	3	0.63	0.281562	0.000009	0.001713	0.051701	2.33
JBM4-178	37	0.5	0.00	0.281043	0.000490	0.001610	0.074118	3.02
JBM4-179	24	1.2	0.00	0.281507	0.000016	0.000760	0.022134	2.35
JBM4-180	13	38.4	0.00	0.281976	0.000012	0.001017	0.034417	1.74
JBM4-181	11	−2.1	0.00	0.282472	0.000008	0.000483	0.014892	1.05
JBM4-182	9	−1.3	0.26	0.282286	0.000011	0.001135	0.036847	1.32
JBM4-183	27	2.7	0.00	0.282435	0.000013	0.005111	0.154393	1.25

Table 2 (*Continued*)

Sample	±1σ	Disc. (%)	Composition of Pb (%)	$^{176}Hf/^{177}Hf$	±1σ	$^{176}Lu/^{177}Hf$	$^{176}Yb/^{177}Hf$	T_{DM} (Ga)
JBM4-184	16	26.3	0.07	0.282754	0.000065	0.002094	0.085922	0.70
JBM4-185	12	−16	0.00	0.282437	0.000009	0.000442	0.016358	1.10
JBM4-186	16	−0.3	0.80	0.281493	0.000009	0.001164	0.038217	2.39
JBM4-188	16	3.1	0.15	0.281518	0.000007	0.000855	0.028191	2.34
JBM4-189	32	5.5	0.00	0.282528	0.000007	0.000859	0.029432	0.99
JBM4-190	19	2.5	0.00	0.281978	0.000007	0.000975	0.035117	1.73
JBM4-191	18	1.2	0.00	0.282287	0.000008	0.000456	0.015613	1.30
JBM4-192	17	0.6	0.00	0.281907	0.000005	0.001180	0.039298	1.84
JBM4-195	27	0.6	0.00	0.281105	0.000012	0.000575	0.019488	2.86
JBM4-195r	45	2.6	0.33	0.281105	0.000012	0.000575	0.019488	2.86
JBM4-196	26	1.2	0.00	0.281046	0.000007	0.000670	0.021893	2.94
JBM4-198	26	11.6	0.00	0.281529	0.000019	0.006089	0.218239	2.69
JBM4-200	21	5.5	0.28	0.282295	0.000012	0.000390	0.012633	1.29
JBM4-201	19	4.8	0.00	0.281386	0.000014	0.001805	0.063164	2.57
JBM4-202	21	6.4	0.00	0.281977	0.000022	0.000488	0.015992	1.71
JBM4-203	9	−3.1	0.00	0.281443	0.000013	0.000869	0.027781	2.44
JBM4-204	14	−2.2	0.00	0.282541	0.000045	0.001261	0.040363	0.98
JBM4-205	11	2.8	0.00	0.282056	0.000012	0.000040	0.001681	1.59
JBM4-206	17	1.6	0.00	0.282387	0.000014	0.000672	0.018976	1.17
JBM4-207	13	−2.1	0.00	0.282473	0.000014	0.000591	0.018952	1.05
JBM4-208	18	−2.8	0.00	0.282588	0.000280	0.000679	0.020097	0.90
JBM4-209	25	−1.9	0.00	0.282399	0.000160	0.001445	0.044318	1.18
JBM4-210	13	−5.6	0.00	0.282195	0.000012	0.000511	0.014769	1.42
JBM4-211	10	−3.4	0.00	0.282309	0.000014	0.000994	0.030668	1.29
JBM4-212	8	2.4	0.00	0.282436	0.000011	0.000516	0.015963	1.10
JBM4-214	16	0.6	0.00	0.281430	0.000010	0.000242	0.007000	2.41
JBM4-215	25	0.7	0.00	0.282409	0.000014	0.000706	0.020881	1.14
JBM4-216	12	1.8	0.00	0.282334	0.000011	0.000353	0.010071	1.23
JBM4-216r	14	2.7	0.00	0.282334	0.000011	0.000353	0.010071	1.23
JBM4-217	14	4.3	0.12	0.282044	0.000012	0.000976	0.031301	1.64
JBM4-218	20	8.8	0.00	0.282211	0.000014	0.000615	0.019116	1.41
JBM4-219	7	−1	0.26	0.282495	0.000017	0.002195	0.078388	1.07
JBM4-219r	10	3.9	0.00	0.282495	0.000017	0.002195	0.078388	1.07
JBM4-220	10	27.2	0.76	0.281997	0.000017	0.002310	0.074701	1.77
JBM4-221	23	1.5	0.00	0.281540	0.000015	0.001260	0.035492	2.33
JBM4-222	19	−0.4	0.00	0.281618	0.000018	0.001710	0.047304	2.25
JBM4-223	12	−0.7	0.00	0.282112	0.000011	0.001309	0.042552	1.57
JBM4-224	9	8.4	0.02	0.281896	0.000013	0.001519	0.046224	1.87
JBM4-226	19	6.8	0.40	0.282526	0.000014	0.001624	0.050360	1.01
JBM4-227	8	−1	0.00	0.282451	0.000012	0.000234	0.007979	1.07
JBM4-227C	16	1.8	0.00	0.282451	0.000012	0.000234	0.007979	1.07
JBM4-228	16	1.6	0.00	0.282001	0.000020	0.001723	0.049004	1.74
JBM4-229	14	0.8	0.00	0.281659	0.000012	0.001748	0.053139	2.20
JBM4-230	11	1.9	0.00	0.282056	0.000036	0.000942	0.029150	1.63
JBM5-001	29	13.4	0.00	0.281594	0.000008	0.000721	0.027622	2.23
JBM5-003	34	5.6	0.00	0.281587	0.000012	0.001714	0.068244	2.30
JBM5-005	41	4	0.00	0.281652	0.000007	0.001691	3.000000	2.21
JBM5-006	6	70	0.00	0.282457	0.000012	0.001995	0.091825	1.12
JBM5-007	30	7	0.00	0.281619	0.000009	0.001162	0.048039	2.22
JBM5-013	29	3	0.11	0.281605	0.000007	0.001176	0.049393	2.24
JBM5-015	32	0.6	0.00	0.281307	0.000008	0.000507	0.022352	2.59
JBM5-016	35	−2.7	0.45	0.281539	0.000007	0.000965	0.043368	2.32
JBM5-022	27	2.1	0.08	0.281787	0.000013	0.001277	0.057608	2.00
JBM5-029	30	−0.5	0.00	0.281535	0.000010	0.001109	0.049711	2.33
JBM5-034	28	−2.7	0.00	0.281554	0.000008	0.002416	0.113301	2.39
JBM5-039	34	0.5	0.00	0.281543	0.000009	0.000946	0.040050	2.31
JBM5-040	24	0.6	0.00	0.281574	0.000017	0.001410	0.056928	2.30
JBM5-043	26	1.2	0.00	0.281596	0.000012	0.001203	0.050219	2.25
JBM5-049	30	1.2	0.00	0.281491	0.000007	0.001320	0.055363	2.40
JBM5-052	69	3.2	0.00	0.281511	0.000008	0.000764	0.032704	2.34
JBM5-056	34	7.9	0.00	0.281110	0.000014	0.000362	0.016243	2.84
JBM5-058	44	1.4	0.00	0.281645	0.000007	0.001190	0.053352	2.19
JBM5-060	27	3.6	0.09	0.281557	0.000006	0.000372	0.015703	2.26
JBM5-085	51	2	0.32	0.280743	0.000011	0.000843	0.033421	3.35
JBM5-103	31	−0.6	0.00	0.281418	0.000008	0.000686	0.030593	2.46
JBM5-121	47	0.3	0.00	0.281250	0.000025	0.001495	0.063040	2.73
JBM5-125	44	3.2	0.36	0.281089	0.000009	0.000468	0.019494	2.87
JBM5-157	30	6.7	0.00	0.281195	0.000006	0.000876	0.033822	2.76
JBM5-181	65	10	0.00	0.281191	0.000014	0.003805	0.219044	3.00

Sample	T_{DM} crustal	Hfi	ε_{Hf}	Morphology	Structure	Modelled rock type
JBM4-001	1.37	0.282333	12.03	3	Diffuse	Granitoid 70–75% SiO_2
JBM4-002	1.24	0.282383	9.89	4	No zoning	Mafic rock
JBM4-003	2.65	0.281513	−2.54	4	No zoning	Granitoid 70–75% SiO_2

Table 2 (*Continued*)

Sample	T_{DM} crustal	Hfi	ε_{Hf}	Morphology	Structure	Modelled rock type
JBM4-004	1.94	0.282079	−2.04	4	Diffuse	Granitoid 70–75% SiO_2
JBM4-005	1.27	0.282498	4.23	3	Diffuse	Granitoid <65% SiO_2
JBM4-006	2.72	0.281226	5.52	4	No zoning	Granitoid <65% SiO_2
JBM4-007	1.21	0.282518	5.32	3	Oscillatory	Granitoid <65% SiO_2
JBM4-008	1.02	0.282587	8.93	4	Diffuse	Granitoid 70–75% SiO_2
JBM4-009	2.39	0.281663	−3.21	4	Diffuse	Mafic rock
JBM4-010	1.73	0.282161	2.15	4	Oscillatory	Granitoid 70–75% SiO_2
JBM4-011	1.32	0.282489	2.84	4	No zoning	Mafic rock
JBM4-013	1.82	0.282216	−3.68	3	Oscillatory	Granitoid 70–75% SiO_2
JBM4-013C	1.81	0.282215	−3.24	3	Oscillatory	Granitoid 70–75% SiO_2
JBM4-015	2.66	0.281484	−1.05	2	Oscillatory	Granitoid <65% SiO_2
JBM4-016	1.46	0.282288	5.90	4	No zoning	Mafic rock
JBM4-017	2.67	0.281479	−2.36	4	No zoning	Mafic rock
JBM4-019	1.44	0.282382	2.99	3	Diffuse	Granitoid 70–75% SiO_2
JBM4-021	2.43	0.281828	−5.69	4	Oscillatory	Granitoid <65% SiO_2
JBM4-023	1.23	0.282506	5.10	4	No zoning	Carbonatite
JBM4-024	1.18	0.282506	6.83	3	No zoning	Mafic rock
JBM4-025	1.63	0.282444	−6.73	3	Oscillatory	Granitoid <65% SiO_2
JBM4-027	2.11	0.281995	−4.48	2	No zoning	Granitoid 70–75% SiO_2
JBM4-028	1.44	0.282284	6.68	4	No zoning	Granitoid 70–75% SiO_2
JBM4-029	2.02	0.282061	−4.29	3	Diffuse	Mafic rock
JBM4-030	1.47	0.282290	5.71	3	No zoning	Granitoid 70–75% SiO_2
JBM4-031	2.34	0.281640	2.43	3	No zoning	Mafic rock
JBM4-032	3.09	0.281054	−0.47	4	Oscillatory	Granitoid 70–75% SiO_2
JBM4-032C	3.35	0.281054	−0.40	4	Oscillatory	Granitoid 70–75% SiO_2
JBM4-033	2.65	0.281501	−3.84	1	Oscillatory	Granitoid <65% SiO_2
JBM4-034	1.31	0.282480	3.32	4	Diffuse	Granitoid 70–75% SiO_2
JBM4-035	1.65	0.282325	17.35	4	No zoning	Granitoid <65% SiO_2
JBM4-036	2.01	0.282043	−3.03	4	Oscillatory	Granitoid 70–75% SiO_2
JBM4-037	1.29	0.282463	4.89	2	Laminated	Mafic rock
JBM4-038	1.38	0.282367	5.92	4	Diffuse	Mafic rock
JBM4-039	2.63	0.281497	−2.09	3	Oscillatory	Granitoid 70–75% SiO_2
JBM4-040	1.87	0.282205	−4.90	3	Diffuse	Granitoid <65% SiO_2
JBM4-041	0.39	0.282514	33.87	4	Diffuse	Syenite
JBM4-042	1.56	0.282260	3.92	4	No zoning	Granitoid <65% SiO_2
JBM4-043	1.30	0.282458	4.79	3	Diffuse	Granitoid 70–75% SiO_2
JBM4-044	3.46	0.280869	−6.42	3	No zoning	Granitoid 70–75% SiO_2
JBM4-045	1.74	0.282255	−2.45	3	Oscillatory	Granitoid <65% SiO_2
JBM4-046	3.07	0.281348	−7.82	3	Oscillatory	Granitoid 70–75% SiO_2
JBM4-047	3.33	0.281157	−11.81	4	No zoning	Granitoid <65% SiO_2
JBM4-048	2.73	0.281453	−3.38	2	Diffuse	Granitoid 70–75% SiO_2
JBM4-050	2.63	0.281476	−1.09	2	Oscillatory	Granitoid <65% SiO_2
JBM4-051	1.20	0.282527	5.45	3	Diffuse	Granitoid <65% SiO_2
JBM4-052	1.14	0.282551	6.32	4	No zoning	Mafic rock
JBM4-053	3.01	0.281068	2.12	3	Oscillatory	Granitoid <65% SiO_2
JBM4-054	2.71	0.281490	−3.96	3	Oscillatory	Granitoid 70–75% SiO_2
JBM4-055	2.64	0.281488	−1.46	3	No zoning	Granitoid 70–75% SiO_2
JBM4-056	1.06	0.282574	8.16	3	Diffuse	Granitoid 70–75% SiO_2
JBM4-057	2.51	0.281570	1.51	3	No zoning	Mafic rock
JBM4-058	2.14	0.281979	−4.89	4	No zoning	Granitoid <65% SiO_2
JBM4-059	2.80	0.281391	−3.79	4	No zoning	Granitoid <65% SiO_2
JBM4-060	2.79	0.281418	−3.91	3	Diffuse	Granitoid 70–75% SiO_2
JBM4-061	1.99	0.282103	−4.90	4	No zoning	Granitoid <65% SiO_2
JBM4-062	1.95	0.282297	−12.21	3	No zoning	Syenite Monzonite
JBM4-063	3.05	0.281566	−19.46	4	No zoning	Granitoid <65% SiO_2
JBM4-064	1.23	0.282522	4.37	4	No zoning	Mafic rock
JBM4-066	2.28	0.281920	−6.60	5	No zoning	Granitoid <65% SiO_2
JBM4-067	2.59	0.281767	−11.50	4	No zoning	Granitoid <65% SiO_2
JBM4-069	2.22	0.281914	−3.01	4	No zoning	Granitoid 70–75% SiO_2
JBM4-070	1.72	0.282289	−3.23	3	No zoning	Granitoid 70–75% SiO_2
JBM4-071	2.56	0.281524	−0.88	3	Oscillatory	Granitoid 70–75% SiO_2
JBM4-072	3.27	0.281551	−28.23	4	No zoning	Granitoid 70–75% SiO_2
JBM4-073	1.62	0.282227	6.41	4	No zoning	Granitoid <65% SiO_2
JBM4-074	2.07	0.282009	−3.20	3	Oscillatory	Granitoid <65% SiO_2
JBM4-075	1.21	0.282468	7.59	3	Diffuse	Mafic rock
JBM4-077	1.54	0.282249	5.52	3	Oscillatory	Granitoid 70–75% SiO_2
JBM4-078	1.81	0.282248	−4.51	2	Diffuse	Mafic rock
JBM4-080	2.01	0.282063	20.56	1	Diffuse	Mafic rock
JBM4-082	1.45	0.282412	10.41	3	No zoning	Granitoid 70–75% SiO_2
JBM4-083	1.46	0.282292	6.00	3	No zoning	Granitoid <65% SiO_2
JBM4-084	2.61	0.281511	−2.03	3	No zoning	Granitoid <65% SiO_2
JBM4-086	1.97	0.282050	−1.80	4	Laminated	Granitoid 70–75% SiO_2
JBM4-087	1.68	0.282200	4.29	3	No zoning	Mafic rock
JBM4-088	2.96	0.281331	−7.09	4	No zoning	Granitoid <65% SiO_2
JBM4-089	2.61	0.281529	−0.58	1	Oscillatory	Granitoid <65% SiO_2

Table 2 (*Continued*)

Sample	T_{DM} crustal	Hfi	ε_{Hf}	Morphology	Structure	Modelled rock type
JBM4-090C	1.51	0.282263	5.91	3	Diffuse	Mafic rock
JBM4-090r	1.43	0.282258	10.25	3	Diffuse	Mafic rock
JBM4-092	2.00	0.282032	−2.18	2	Diffuse	Granitoid 70–75% SiO_2
JBM4-093	3.47	0.280895	−6.73	4	No zoning	Granitoid <65% SiO_2
JBM4-094	1.56	0.282361	−0.38	4	No zoning	Granitoid 70–75% SiO_2
JBM4-095	2.76	0.281509	−3.45	4	No zoning	Granitoid <65% SiO_2
JBM4-096	1.25	0.282506	4.28	4	No zoning	Granitoid <65% SiO_2
JBM4-097	2.19	0.281942	−2.29	4	No zoning	Mafic rock
JBM4-098	2.39	0.281859	−8.91	5	No zoning	Mafic rock
JBM4-099	2.98	0.281421	0.03	1	Oscillatory	Granitoid 70–75% SiO_2
JBM4-100	1.52	0.282255	6.14	4	No zoning	Granitoid <65% SiO_2
JBM4-101	1.32	0.282491	2.63	3	No zoning	Mafic rock
JBM4-102	3.44	0.280982	−1.78	4	Diffuse	Granitoid 70–75% SiO_2
JBM4-103	1.93	0.282093	−2.25	2	Oscillatory	Granitoid <65% SiO_2
JBM4-104	2.34	0.281893	−8.43	3	Diffuse	Granitoid 70–75% SiO_2
JBM4-105	1.53	0.282387	−0.68	4	Diffuse	Granitoid <65% SiO_2
JBM4-106	2.70	0.281455	−2.18	3	Oscillatory	Granitoid <65% SiO_2
JBM4-107	2.67	0.281470	−1.21	3	Diffuse	Granitoid <65% SiO_2
JBM4-108	3.96	0.280900	−4.59	3	Diffuse	Granitoid 70–75% SiO_2
JBM4-109	3.23	0.281522	6.05	2	Diffuse	Granitoid 70–75% SiO_2
JBM4-110	2.78	0.281390	−2.40	4	Oscillatory	Granitoid <65% SiO_2
JBM4-111	1.29	0.282499	3.30	3	Laminated	Granitoid 70–75% SiO_2
JBM4-112	1.38	0.282443	2.34	4	No zoning	Granitoid <65% SiO_2
JBM4-112r	1.37	0.282443	2.73	4	No zoning	Granitoid <65% SiO_2
JBM4-113	1.58	0.282338	−0.10	4	No zoning	Mafic rock
JBM4-114	3.09	0.280966	1.87	4	Diffuse	Granitoid <65% SiO_2
JBM4-115	2.43	0.281574	1.15	3	Oscillatory	Granitoid <65% SiO_2
JBM4-116	1.49	0.282406	20.25	4	Laminated	Granitoid >75% SiO_2
JBM4-117	2.43	0.281598	2.28	3	No zoning	Granitoid 70–75% SiO_2
JBM4-118	1.15	0.282424	12.00	3	Diffuse	Granitoid 70–75% SiO_2
JBM4-119	2.02	0.282038	−1.87	4	Oscillatory	Granitoid <65% SiO_2
JBM4-120	1.34	0.282430	4.37	4	Oscillatory	Granitoid <65% SiO_2
JBM4-121	1.64	0.282251	12.30	2	Laminated	Granitoid 70–75% SiO_2
JBM4-122	1.26	0.282473	5.57	4	Diffuse	Granitoid <65% SiO_2
JBM4-123	1.05	0.282569	8.79	4	Oscillatory	Granitoid <65% SiO_2
JBM4-124	1.14	0.282436	11.69	4	No zoning	Mafic rock
JBM4-125	1.18	0.282512	6.79	4	Diffuse	Granitoid 70–75% SiO_2
JBM4-127	1.31	0.282477	3.55	4	Oscillatory	Mafic rock
JBM4-128	2.74	0.281511	−0.22	1	Oscillatory	Granitoid 70–75% SiO_2
JBM4-129	2.52	0.281545	−0.39	1	Oscillatory	Granitoid 70–75% SiO_2
JBM4-131	2.15	0.281971	−4.71	1	Laminated	Mafic rock
JBM4-132	2.66	0.281488	−2.35	3	Diffuse	Mafic rock
JBM4-134	1.29	0.282341	9.89	2	No zoning	Granitoid 70–75% SiO_2
JBM4-135	1.49	0.282276	5.55	2	Oscillatory	Granitoid 70–75% SiO_2
JBM4-136	1.56	0.282303	2.09	3	Laminated	Granitoid 70–75% SiO_2
JBM4-137	1.46	0.282280	6.72	3	No zoning	Granitoid 70–75% SiO_2
JBM4-138	2.36	0.281599	4.41	3	Oscillatory	Mafic rock
JBM4-139	2.22	0.281933	−5.20	4	Diffuse	Granitoid <65% SiO_2
JBM4-140	2.62	0.281502	−2.33	4	Diffuse	Granitoid 70–75% SiO_2
JBM4-141	2.65	0.281495	−1.85	4	Oscillatory	Granitoid 70–75% SiO_2
JBM4-142	2.71	0.281477	−2.69	4	Oscillatory	Granitoid 70–75% SiO_2
JBM4-143	3.11	0.281003	1.41	3	Metamict	Granitoid 70–75% SiO_2
JBM4-144	2.44	0.281835	−8.22	4	No zoning	Mafic rock
JBM4-145	1.69	0.282288	−2.17	3	No zoning	Granitoid <65% SiO_2
JBM4-146	1.36	0.282394	5.31	3	Diffuse	Granitoid <65% SiO_2
JBM4-147	1.97	0.282086	−3.48	4	Diffuse	Granitoid 70–75% SiO_2
JBM4-148	5.28	0.280042	−35.00	3	Oscillatory	Granitoid 70–75% SiO_2
JBM4-149	1.68	0.282193	2.42	3	Diffuse	Granitoid 70–75% SiO_2
JBM4-150	3.13	0.281039	−1.06	4	No zoning	Granitoid <65% SiO_2
JBM4-151	1.10	0.282552	7.72	3	No zoning	Granitoid 70–75% SiO_2
JBM4-152	1.03	0.282554	10.32	3	Laminated	Granitoid 70–75% SiO_2
JBM4-153	2.35	0.281600	3.06	1	Oscillatory	Mafic rock
JBM4-154	1.40	0.282315	6.97	4	Diffuse	Granitoid 70–75% SiO_2
JBM4-155	2.70	0.281470	−2.65	4	Diffuse	Mafic rock
JBM4-156	0.93	0.282621	10.79	1	Diffuse	Granitoid 70–75% SiO_2
JBM4-157	2.27	0.281665	4.28	2	No zoning	Granitoid <65% SiO_2
JBM4-159r	1.48	0.282399	0.91	4	Diffuse	Granitoid 70–75% SiO_2
JBM4-160	2.15	0.281961	−4.84	3	Diffuse	Granitoid 70–75% SiO_2
JBM4-162	2.00	0.282043	−1.93	3	No zoning	Mafic rock
JBM4-163	2.55	0.281526	−0.55	2	Diffuse	Granitoid 70–75% SiO_2
JBM4-164	2.68	0.281716	−12.73	3	No zoning	Syenite/Monzonite
JBM4-165	2.93	0.281733	−23.67	4	No zoning	Mafic rock
JBM4-166	3.25	0.281272	11.61	1	Oscillatory	Granitoid >75% SiO_2
JBM4-167	1.86	0.282135	0.46	4	No zoning	Granitoid 70–75% SiO_2
JBM4-168	3.09	0.281041	2.18	3	Diffuse	Mafic rock

Table 2 (*Continued*)

Sample	T_{DM} crustal	Hfi	ε_{Hf}	Morphology	Structure	Modelled rock type
JBM4-169	2.71	0.281432	−3.81	3	Oscillatory	Granitoid 70–75% SiO_2
JBM4-170	2.74	0.281437	−3.45	2	Diffuse	Granitoid 70–75% SiO_2
JBM4-170r	2.75	0.281437	−3.45	2	Diffuse	Granitoid 70–75% SiO_2
JBM4-171	1.53	0.282255	5.84	3	No zoning	Granitoid <65% SiO_2
JBM4-172	2.87	0.281503	−9.69	4	Diffuse	Mafic rock
JBM4-173	2.61	0.281498	−1.96	1	Oscillatory	Granitoid 70–75% SiO_2
JBM4-174	1.39	0.282320	7.92	3	No zoning	Mafic rock
JBM4-175	1.34	0.282391	6.06	4	Laminated	Mafic rock
JBM4-176	2.14	0.281980	−4.85	3	Diffuse	Granitoid <65% SiO_2
JBM4-177	2.63	0.281500	−2.37	4	Diffuse	Mafic rock
JBM4-177r	2.64	0.281499	−1.70	4	Diffuse	Mafic rock
JBM4-178	3.28	0.280959	−3.06	3	Oscillatory	Granitoid 70–75% SiO_2
JBM4-179	2.65	0.281479	−1.73	2	Oscillatory	Granitoid <65% SiO_2
JBM4-180	2.23	0.281947	4.64	3	Diffuse	Granitoid 70–75% SiO_2
JBM4-181	1.36	0.282467	2.26	4	No zoning	Granitoid <65% SiO_2
JBM4-182	1.52	0.282264	5.06	4	Diffuse	Mafic rock
JBM4-183	1.36	0.282332	8.20	4	No zoning	Granitoid >75% SiO_2
JBM4-184	0.12	0.282665	46.31	4	Diffuse	Granitoid 70–75% SiO_2
JBM4-185	1.40	0.282432	2.44	2	Oscillatory	Mafic rock
JBM4-186	2.78	0.281453	−5.86	1	Oscillatory	Granitoid 70–75% SiO_2
JBM4-188	2.67	0.281486	−1.95	2	Diffuse	Mafic rock
JBM4-189	1.20	0.282517	5.68	3	Diffuse	Mafic rock
JBM4-190	2.18	0.281958	−4.90	3	No zoning	Granitoid 70–75% SiO_2
JBM4-191	1.71	0.282281	−2.54	4	No zoning	Mafic rock
JBM4-192	2.36	0.281884	−8.97	3	No zoning	Granitoid 70–75% SiO_2
JBM4-195	3.03	0.281075	1.20	3	Oscillatory	Granitoid <65% SiO_2
JBM4-195r	3.14	0.281076	−1.65	3	Oscillatory	Granitoid <65% SiO_2
JBM4-196	3.19	0.281011	−1.57	4	No zoning	Mafic rock
JBM4-198	3.02	0.281274	−3.84	2	Oscillatory	Granitoid 70–75% SiO_2
JBM4-200	1.47	0.282287	7.27	4	No zoning	Granitoid <65% SiO_2
JBM4-201	3.03	0.281318	−7.13	4	No zoning	Granitoid 70–75% SiO_2
JBM4-202	2.18	0.281967	−4.49	4	Diffuse	Granitoid <65% SiO_2
JBM4-203	3.34	0.281426	−25.22	3	No zoning	Granitoid <65% SiO_2
JBM4-204	1.15	0.282524	7.09	3	No zoning	Mafic rock
JBM4-205	2.19	0.282055	−10.12	5	No zoning	Granitoid <65% SiO_2
JBM4-206	1.30	0.282374	8.21	3	Diffuse	Mafic rock
JBM4-207	1.32	0.282466	3.63	4	Oscillatory	Granitoid <65% SiO_2
JBM4-208	0.81	0.282574	16.42	3	No zoning	Granitoid <65% SiO_2
JBM4-209	1.41	0.282376	4.33	2	No zoning	Mafic rock
JBM4-210	1.64	0.282185	2.97	4	Diffuse	Granitoid <65% SiO_2
JBM4-211	1.59	0.282294	1.37	4	Oscillatory	Granitoid 70–75% SiO_2
JBM4-212	1.41	0.282430	2.06	3	Diffuse	Granitoid <65% SiO_2
JBM4-214	2.75	0.281421	−3.17	3	No zoning	Granitoid <65% SiO_2
JBM4-215	1.23	0.282395	10.10	3	Laminated	Granitoid <65% SiO_2
JBM4-216	1.37	0.282327	8.17	5	Diffuse	Granitoid <65% SiO_2
JBM4-216r	1.34	0.282326	9.34	5	Diffuse	Granitoid <65% SiO_2
JBM4-217	2.07	0.282025	−3.48	4	Diffuse	Granitoid 70–75% SiO_2
JBM4-218	1.81	0.282202	−2.77	3	No zoning	Mafic rock
JBM4-219	1.26	0.282463	6.07	3	Oscillatory	Granitoid >75% SiO_2
JBM4-219r	1.27	0.282465	5.34	3	Oscillatory	Granitoid >75% SiO_2
JBM4-220	2.28	0.281958	−9.03	3	Oscillatory	Granitoid >75% SiO_2
JBM4-221	2.63	0.281493	−1.57	3	Oscillatory	Mafic rock
JBM4-222	2.48	0.281551	2.60	2	Diffuse	Mafic rock
JBM4-223	1.90	0.282086	−0.88	1	No zoning	Granitoid >75% SiO_2
JBM4-224	2.42	0.281866	−8.72	4	Laminated	Mafic rock
JBM4-226	1.13	0.282500	9.11	3	Diffuse	Mafic rock
JBM4-227	1.34	0.282448	3.80	4	Diffuse	Granitoid <65% SiO_2
JBM4-227C	1.33	0.282448	3.99	4	Diffuse	Granitoid <65% SiO_2
JBM4-228	2.18	0.281968	−6.00	3	Diffuse	Mafic rock
JBM4-229	2.46	0.281597	−0.15	4	Oscillatory	Mafic rock
JBM4-230	1.99	0.282036	−1.68	3	Diffuse	Mafic rock
JBM5-001	2.45	0.281564	6.97	3	No zoning	Granitoid <65% SiO_2
JBM5-003	2.59	0.281522	0.24	2	Diffuse	Granitoid 70–75% SiO_2
JBM5-005	2.45	0.281589	1.62	1	No zoning	Granitoid 70–75% SiO_2
JBM5-006	1.38	0.282379	32.04	4	Oscillatory	Granitoid 70–75% SiO_2
JBM5-007	2.49	0.281575	2.03	2	No zoning	Granitoid 70–75% SiO_2
JBM5-013	2.50	0.281561	0.90	4	Oscillatory	Granitoid 70–75% SiO_2
JBM5-015	2.97	0.281287	−5.38	5	No zoning	Granitoid <65% SiO_2
JBM5-016	2.58	0.281503	−1.51	2	Oscillatory	Mafic rock
JBM5-022	2.11	0.281740	6.86	3	No zoning	Mafic rock
JBM5-029	2.63	0.281494	−2.18	2	Oscillatory	Granitoid 70–75% SiO_2
JBM5-034	2.67	0.281465	−3.10	3	Oscillatory	Granitoid 70–75% SiO_2
JBM5-039	2.61	0.281508	−1.73	2	No zoning	Granitoid 70–75% SiO_2
JBM5-040	2.58	0.281522	−1.21	2	Oscillatory	Granitoid 70–75% SiO_2
JBM5-043	2.51	0.281552	0.11	2	Oscillatory	Granitoid 70–75% SiO_2

Table 2 (*Continued*)

Sample	T_{DM} crustal	Hfi	ε_{Hf}	Morphology	Structure	Modelled rock type
JBM5-049	2.75	0.281442	−3.70	4	No zoning	Syenite
JBM5-052	2.70	0.281483	−3.05	4	No zoning	Granitoid 70–75% SiO_2
JBM5-056	3.09	0.281091	2.37	4	Diffuse	Granitoid <65% SiO_2
JBM5-058	2.40	0.281601	1.94	3	Oscillatory	Granitoid 70–75% SiO_2
JBM5-060	2.49	0.281543	2.20	4	No zoning	Granitoid <65% SiO_2
JBM5-085	3.42	0.280688	3.17	5	No zoning	Granitoid 70–75% SiO_2
JBM5-103	2.73	0.281390	−1.69	4	No zoning	Granitoid <65% SiO_2
JBM5-121	2.59	0.281162	12.22	3	No zoning	Granitoid 70–75% SiO_2
JBM5-125	3.08	0.281065	0.40	4	No zoning	Granitoid <65% SiO_2
JBM5-157	2.93	0.281149	4.52	3	No zoning	Granitoid 70–75% SiO_2
JBM5-181	3.34	0.280998	−3.07	4	Diffuse	Granitoid 70–75% SiO_2

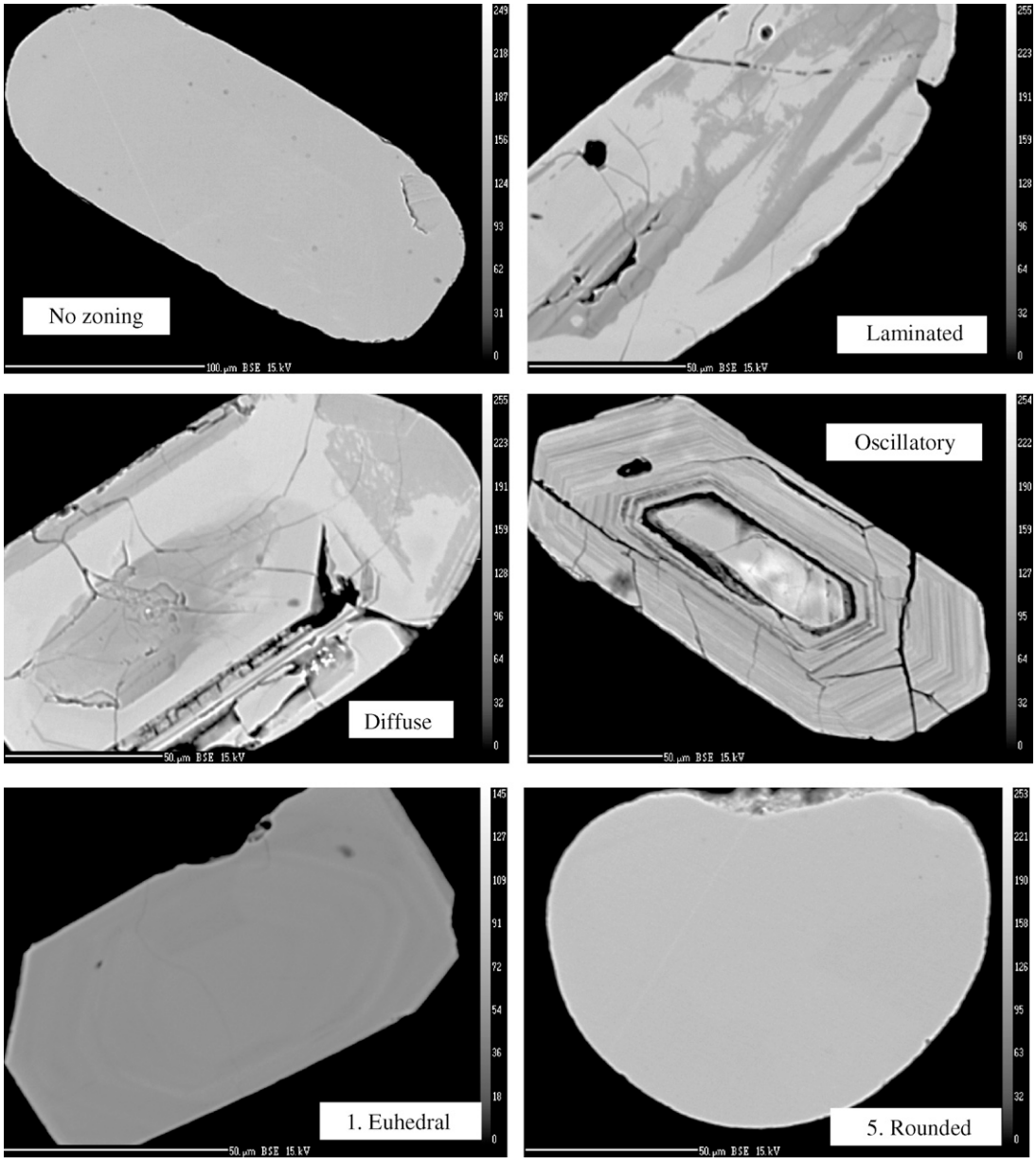

Fig. 3. Representative backscattered electron images showing internal structure and morphology (end members 1 and 5) of zircons.

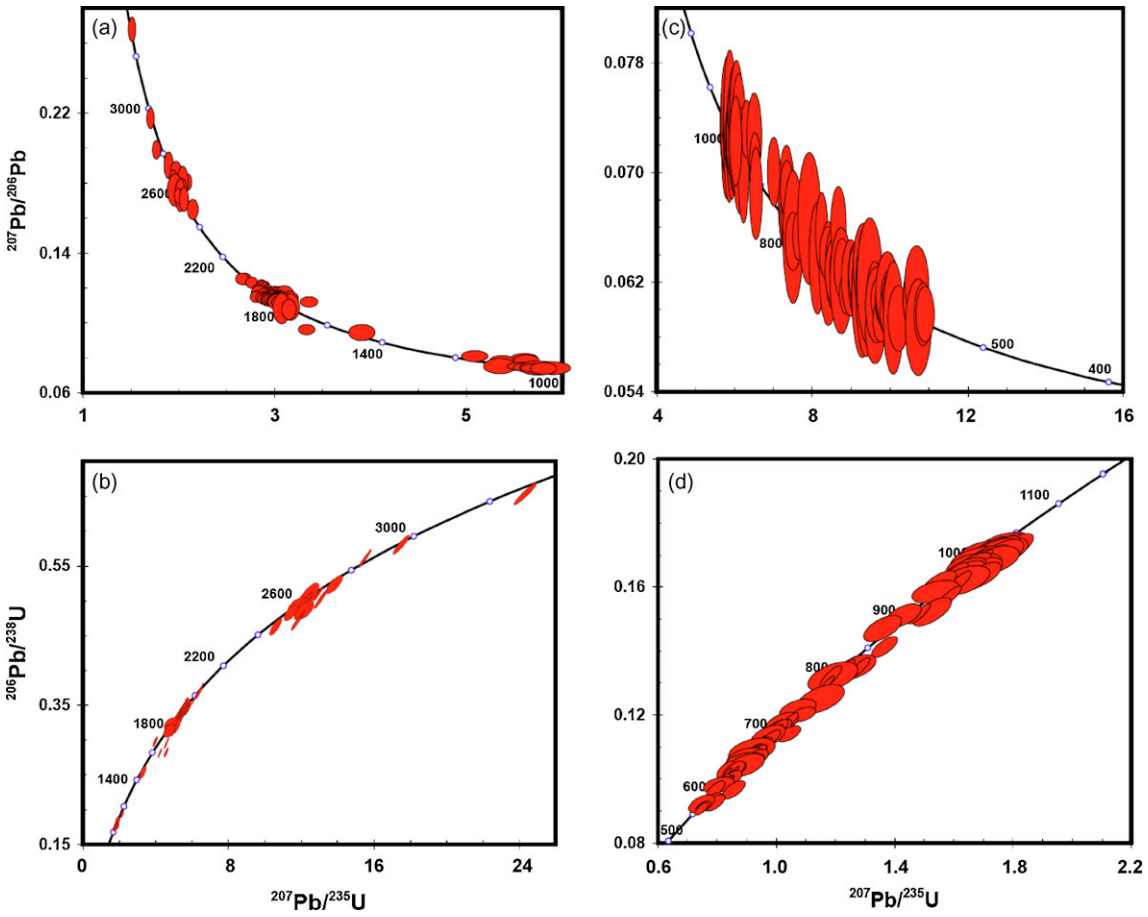

Fig. 4. U–Pb data in inverse Concordia (a and c) and Concordia (b and d) plots with $^{207}Pb/^{206}Pb$ ages for grains older than 1.0 Ga and $^{206}Pb/^{238}U$ ages for younger grains; ellipses show 1σ errors.

trace- and minor-element composition. The trace- and minor-element data are acquired during the EMP (Hf, Y), U–Pb (U, Th) and Hf-isotope (Yb, Lu) analyses of zircon. This approach is used here to characterise the host rock for the zircons of different ages. Most late Archean zircons were derived from low-SiO_2 (<65%) and high-SiO_2 (70–75%) granitoids and a few from mafic rocks (Table 2, Fig. 7). This indicates that the Archean magmatism in the region was mostly felsic, and is consistent with the high relative abundance of granitic plutons of this age known in the region, compared to mafic rocks (e.g. Cahen et al., 1984).

Most of the Paleoproterozoic zircon grains were derived from high-SiO_2 (70–75% SiO_2) granitoids, with a small contribution from low-SiO_2 (<65% SiO_2) granitoids, mafic and alkaline (e.g. syenitic) rocks (Table 2; Fig. 7). During Mesoproterozoic and Neoproterozoic times, there was bimodal magmatism in the region. This is shown by the presence of zircons derived from both low-SiO_2 (<65% SiO_2) and high-SiO_2 (70–75% SiO_2) granitoids and from mafic sources, with very few from >75% SiO_2 granitoids or alkaline rocks (Fig. 7).

4.3. Hf-isotope data

Hf-isotopes in zircon of known U–Pb ages may provide information on the source of the magma from which the zircon crystallised (Griffin et al., 2004). The fact that zircon is the major reservoir of Hf in most rocks and is very refractory, makes the resetting of the Hf-isotope composition during metamorphic and magmatic events very difficult (Griffin et al., 2006). This allows the use of Hf-isotopes in zircon for the understanding of the evolution of the crust. Fig. 8a shows the relationship between the age (U/Pb) and initial Hf-isotope composition of the zircons. In this plot, zircons plotting between the Depleted Mantle (DM) and Chondritic Uniform Reservoir (CHUR) lines are considered to be derived from

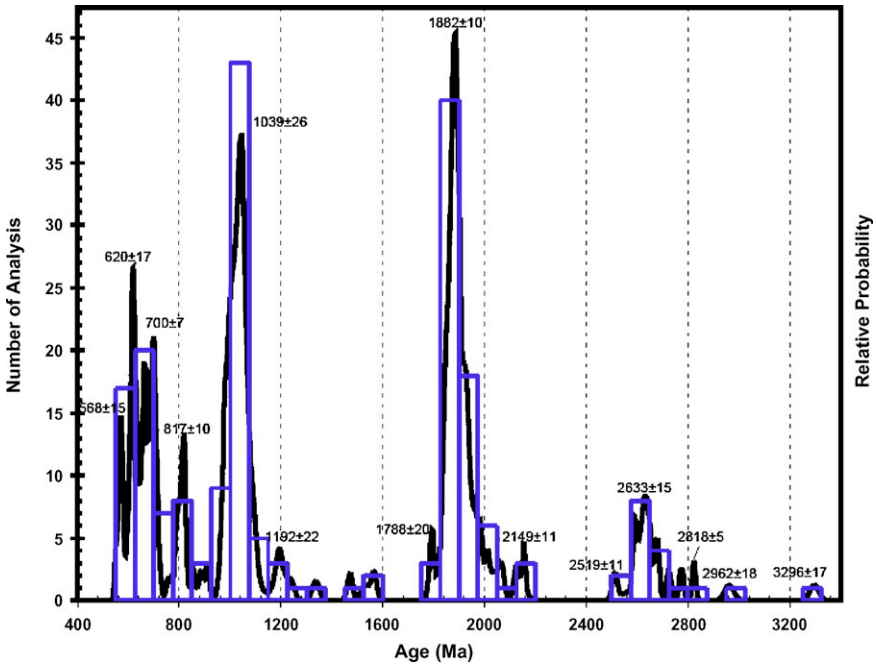

Fig. 5. Probability density plot and histogram of U–Pb zircon data; ages and errors estimated by modelling peaks as Gaussian forms.

relatively juvenile magmas, whereas those that fall below the CHUR line indicate recycling of pre-existing crustal material.

The oldest zircon grain, yielding an age of ~3.3 Ga, lies between the CHUR and DM reference lines (Fig. 8a). This zircon's host magma could represent the oldest juvenile magmatism known in the region. The late Archean zircons are divided into two groups, with most lying below the CHUR reference line. Their model ages indicated that the magma source separated from the DM between 3.4 and 3 Ga. Around 2.5–2.6 Ga, there was a very little input of juvenile material into the crust; few grains plot between CHUR and DM (Fig. 8a). Most of the magmas in that period (late Archean) may be the recycled products of the Mesoarchean crust as the grains (below the CHUR line) lie close to a line, with a slope represent-

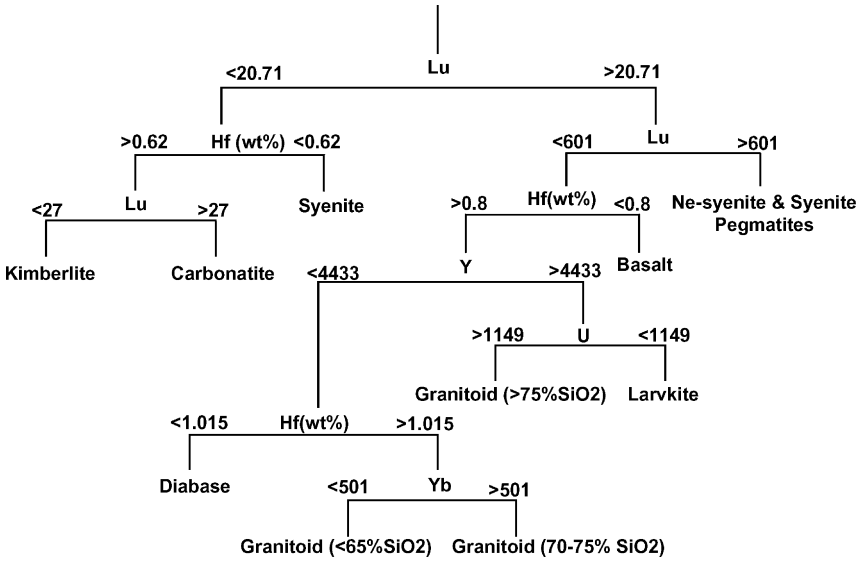

Fig. 6. CART tree for classification of zircons by host-rock type, using trace and minor elements acquired during EMP, U–Pb and Hf-isotope analysis (Belousova et al., 2002).

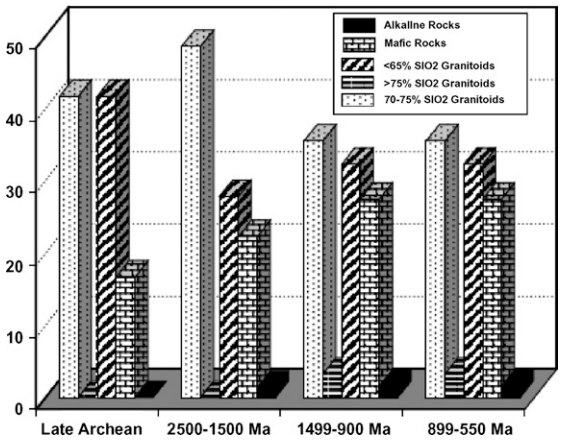

Fig. 7. Relative proportion of zircon host-rock types by age group (Ma).

ing the evolution of the average continental crust, which projects back to the ~3.3 Ga zircon (Fig. 8a).

The host magmas of most of the Paleoproterozoic zircons were derived from older crustal material; they lie on or below the CHUR reference line. This suggests that there was little production of juvenile magma during Paleoproterozoic times in the region (Fig. 8a). However, most of the zircons that do indicate a juvenile input (lying between CHUR and DM line, Fig. 8a) were derived from mafic magmatic rocks. Considering that mafic rocks generally have low zircon contents, such mafic rocks may constitute an essential part of the juvenile input during this period (1.8–1.9 Ga, Fig. 8a), and are under-represented in the zircon population sampled.

Mesoproterozoic and Neoproterozoic times are characterised by an important juvenile input into the crust as shown by a large proportion of grains lying between the CHUR and DM reference lines, suggesting a continuous magmatism during this period (Fig. 8a). Some Mesoproterozoic and Neoproterozoic grains lie near the crustal-evolution line extending from the ~3.3 Ga zircon (Fig. 8a), suggesting the continued reworking of a Mesoarchean crust during these periods of time. However, these zircons also have similar $^{176}Hf/^{177}Hf$ to the cluster of grains observed around 1.8 Ga (Paleoproterozoic, Fig. 8a). This suggests that these zircons could be metamorphic, derived from a Paleoproterozoic protolith. The $^{207}Pb/^{206}Pb$ ages of these zircons could be spurious, reflecting non-zero Pb loss during other events between the Paleoproterozoic and the present. Most of these zircons are rounded (classes 4–5 in Fig. 5) and do not show any oscillatory structure characteristic of magmatic zircon, and this would be consistent with a metamorphic origin.

The other group of Mesoproterozoic and Neoproterozoic zircons below the CHUR line could represent a recycling of the 1.8–1.9 Ga juvenile magmatic rocks observed in the Paleoproterozoic population (Fig. 8a). The grains that fall above the DM fall on a line which projects back to the 3.4 Ga crust, but with higher $^{176}Lu/^{177}Hf$ ratio (0.059, Fig. 8a). These three grains are rounded (3–4 scale in Fig. 3) and have diffuse internal structure or do not present any zoning (Table 2). They could be metamorphic zircons derived from an Archean protolith with high $^{176}Lu/^{177}Hf$ (e.g. a garnet-rich rock). Similarly, the zircon above the DM line around 1 Ga could be derived from a $^{176}Lu/^{177}Hf$-rich Paleoproterozoic protolith.

5. Discussion and interpretation

5.1. Archean

The oldest rocks in the region are the 'Haute Lwanyi gneisses' (Congo-Kasai Craton) giving ages of 3487 ± 67 (Rb–Sr; Delhal and Ledent, 1973) and the Sandoa-Kapanga complex (Congo-Kasai Craton) dated at 3086 and 3021 ± 48 Ma (Walraven and Rumvegeri, 1993). The rounded zircon with a ~3.3 Ga age found in this study could be derived from such rocks. Similar Mesoarchean ages (3.1 Ga) have been reported by Kokonyangi et al. (2007) on detrital zircon from the Kibaran rocks in Nzilo (Katanga, Congo). Rainaud et al. (2003) interpreted ages between 3169 and 3225 Ma on a group of xenocrystic zircons as evidence of the presence of a Mesoarchean basement beneath the Lufilian Belt. However, the zircon grain giving the age of ~3.3 Ga is strongly rounded, and the absence of any euhedral grains in the Archean population analysed here suggests that these grains are long-transported and probably recycled.

This ~3.3 Ga zircon may derive from the Congo Craton, and/or could be inherited from Kibaran metasediments, and does not support the presence of an Archean basement beneath the Kundelungu region. This is also indicated by the fact that the Archean population is poorly represented in the zircons analysed here (Fig. 5). However, some younger zircon grains analysed here have low Hf-isotopic ratios indicative of derivation by recycling of an Archean crust in Neoproterozoic time. These zircons lie along a crustal-evolution line that projects back to the ~3.3 Ga zircon (Fig. 8a). However, the fact that these zircons have similar $^{176}Hf/^{177}Hf$ initial ratios to Paleoproterozoic zircons, and their morphology and internal structure, also suggest that they could be metamorphic, and the presence of an Archean crust

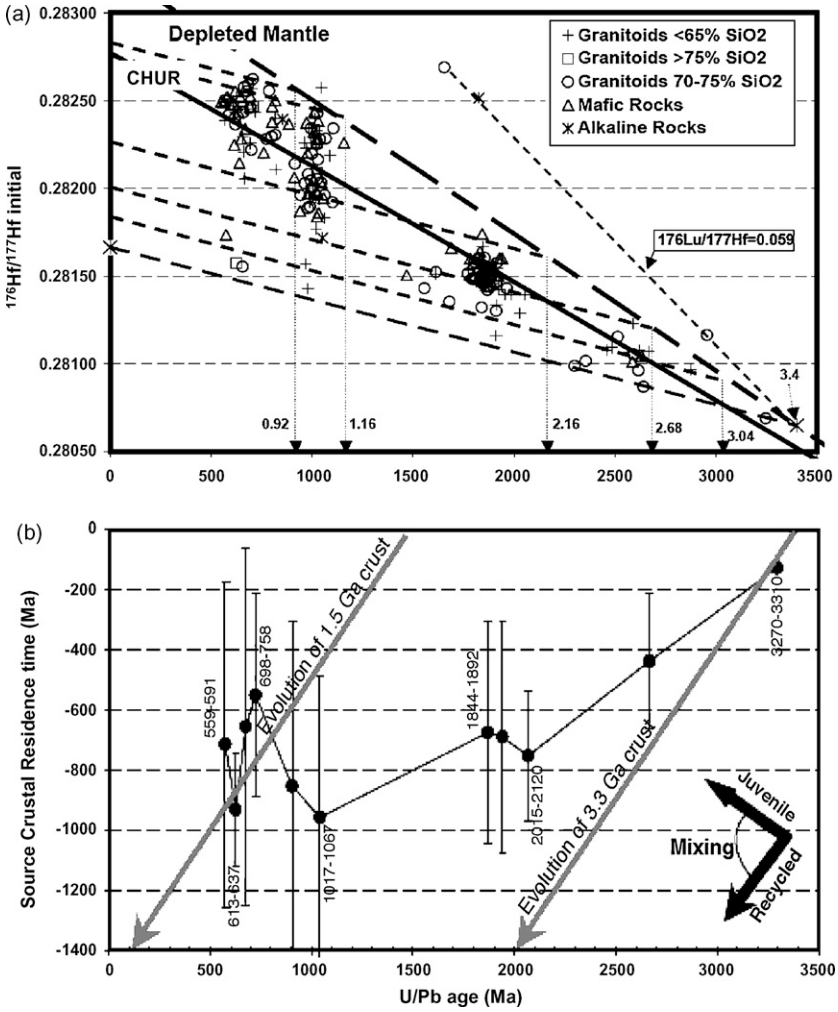

Fig. 8. (a) Age, Hf-isotope and rock-type data for each sample and calculated crustal ages (see Table 2 for details). CHUR: Chondritic Uniform Reservoir. Dashed lines show evolution of crustal volumes with $^{176}Lu/^{177}Hf = 0.015$, corresponding to the average continental crust. (b) Event signature curve. Source crustal residence time is the time from the separation of the source from the Depleted Mantle to the crystallisation of the zircon. In this plot, an upward trend with decreasing age indicates juvenile input, while a downward trend implies reworking of older crust.

during Mesoproterozoic to Neoproterozoic time cannot be clearly demonstrated with these data.

Similarly the 2818 ± 5 Ma zircon population reported here corresponds to the age (2852 ± 46 Ma; Delhal and Liégeois, 1982) of the Sandoa-Kapanga complex (Congo Craton). The late magmatic events in the Congo Craton dated at 2637 ± 33, 2678 ± 23, and 2648 ± 22 Ma and 2593 ± 96 (Delhal et al., 1976; Cahen et al., 1984; Caen-Vachette et al., 1988; Tchameni et al., 2000) correspond to the age range between 2633 ± 15 and 2591 ± 13 Ma defined by zircons analysed here (Fig. 5). This also is similar to a U/Pb zircon age of 2608 ± 14 Ma recorded in the southeastern Irumide Belt (Cox et al., 2002). This late Archean event, which is characterised mostly by felsic magmatism in the Congo-Kasai Craton, involved recycling of a juvenile Mesoarchean crust with little input of juvenile material (Figs. 7 and 8). The small age group observed at 2519 ± 11 could correspond to the magmatic event in NW Zambia dated between 2540 and 2560 Ma by Key et al. (2001).

5.2. Paleoproterozoic

Rainaud et al. (2003) found zircons aged 2297–2114 Ma in the central part of the Lufilian Belt that they interpreted as being derived from the Zimbabwe Craton where ages between 2160 ± 100 and 2120 ± 40 are reported (Master, 1991; Schildlowski and Todt, 1998). The two zircons from this study with ages of 2155 ± 6 and 2125 ± 10 Ma are subrounded and

could be derived from the Zimbabwe Craton, with a long history in the sedimentary cycle.

Lenoir et al. (1994) defined two tectonic events in the Paleoproterozoic Ubendian Belt at 2100–2025 and 1860–1725 Ma, respectively, which led to the formation of a Paleoproterozoic supercontinent (Condie, 2002). These events are represented in our samples by the zircon populations with ages of 2149 ± 11, 1882 ± 10 (the major peak) and 1788 ± 20 Ma. This corresponds also to the age of calc-alkaline magmatism in the Pepa-Lubumba area (northern part of the Katangan belt; 1861 ± 28 Ma; Kabengele et al., 1991). In the Bangweulu Block (Zambia), Vrána et al. (2004) reported ages ranging from 1950 to 1800 Ma, and De Waele and Mapani (2002) and De Waele et al. (2006a,b) also found ages of 2050–1800 Ma in the basement rocks of the northern part of the Irumide Belt in Zambia. The zircons analysed here could then be derived from the Bangweulu Block, the Ubendian Belt and/or the Irumide Belt. Similar Paleoproterozoic ages are found in granitic domes inside the Lufilian Belt that formed part of the Ubendian orogeny.

The Paleoproterozoic magmatism is mostly characterised by recycling of a late Archean to Mesoarchean crust, as also suggested by De Waele et al. (2006a). The Hf-isotopic data suggest that there was a little input of juvenile material during that time. However, as pointed out above, juvenile magmatism during this period may have been mostly mafic and thus could be under-represented in the zircon populations.

5.3. Mesoproterozoic

The small zircon populations yielding ages of 1469 ± 11 and 1339 ± 15 Ma correspond to the timing of the first magmatic cycle in the Kibaran Belt dated between 1.4 and 1.38 Ga (Kokonyangi et al., 2006). The 1192 ± 22 Ma zircon population could correspond to the second post-orogenic event in the northern part of the Kibaran Belt in Burundi (Tack et al., 2002), but such event is not reported in the southern part of the Kibaran Belt (Mitwaba, Katanga) neither in the Irumide Belt. This is correlative to the second magmatic event defined in the Choma-Kalomo Block (Johnson et al., 2005; Bulambo et al., 2004) at ∼1180–1198 Ma. Considering the position of the study area, the zircons dated at 1192 may be derived from the Choma Kalomo Block.

The major Mesoproterozoic zircon population in the Kundelungu data is dated at 1039 ± 26 Ma. Johnson et al. (2005) reported syn to post-tectonic granitoids in the Irumide Belt at 1046 ± 3 and 1020 ± 3 Ma. This could correspond to the magmatic event and metamorphism in the southern Irumide Belt dated at ∼1050 Ma (Johnson et al., 2005, 2006) and represents the Irumide phase (1050–950) defined in the Irumide Belt by De Waele et al. (2006a,b). This large zircon population at 1039 ± 26 Ma thus reflects magmatic events linked with a continental collision between 1250 and 1000 Ma in the Kibaran Belt (Kokonyangi et al., 2004, 2006). The small population found around 950–1000 Ma may then represent the intrusion of tin-garnitoids in the Kibaran Belt.

Kokonyangi et al. (2004) stated that the S-type Kibaran granitoids were derived from melting of metasedimentary Paleoproterozoic rocks and they were associated with mafic magmatism. Our Hf-isotopic data show that some of Mesoproterozoic magmas were derived from a Paleoproterozoic crust, while others represent juvenile material (Fig. 8a), and the trace-element data for these zircons confirm the existence of bimodal magmatism during Mesoproterozoic time in the region (Fig. 7). Based on whole-rock Sm/Nd isotope analysis of the 1350 Ma granites in the Choma-Kalomo Block, Hanson et al. (1988) concluded that the granitoids were not derived from an Archean source (Johnson et al., 2005). Our data confirm that conclusion.

De Waele et al. (2003) proposed that granitoids in Irumide Belt were produced by remelting of an older continental crust due to their highly negative bulk-rock $\varepsilon_{Nd}(t)$ values. However, our data suggest the existence of juvenile magmatism as well as magmas produced from Paleoproterozoic crustal material during this time (Fig. 8a). The derivation of these magmas from Archean crustal materials is questionable due to the morphology, internal structures and $^{176}Hf/^{177}Hf$ initial ratios of the zircons, as discussed above. This bimodal magmatism could be temporally linked to the breakup of Rodinia.

5.4. Neoproterozoic

The opening of the Katangan basin following the break-up of Rodinia is represented by granites and rhyolites dated at 879 Ma (Kafue rhyolites; Hanson et al., 1994), 877 Ma (Nchanga granite; Porada and Berhorst, 2000) and 865 Ma (Lusaka granite; Barr et al., 1977). This event is also witnessed by continental tholeiites and alkaline mafic rocks (not radiometrically dated) known inside the Lufilian Belt (Domes area, Kampunzu et al., 2000). The magmatic activity within the Katangan belt appears to have been continuous during the deposition of the Katangan sediments. Basalts and basaltic andesites found in the Katangan Belt have been dated at 750 ± 5 Ma (Key et al., 2001; Liyungu et al., 2001). Barron et al. (2003) found 745 ± 7.8 and 725 ± 8.6 Ma zircon ages for gabbroic bodies in Solwezi

area in Zambia. These mafic bodies are taken as evidence of extensional magmatism during the deposition of Mwashia Subgroup because they are also found interlayered in Mwashia sediments. The Kibambale mafic rocks that are interstratified within the Mwale Formation (Grand Conglomérat, dated at ∼750 Ma, see Table 1) may represent the continuation of the Mwashia magmatism event. The magmatism during Neoproterozoic times was largely juvenile, but also involved the recycling of older crustal material (Paleoproterozoic and Mesoproterozoic; Fig. 8a).

The different Neoproterozoic zircon ages reported here thus can be related to magmatic activity, from the opening of the Katangan basin to the end of the Lufilian orogeny, supposed to occur at around 540 Ma. John et al. (2004) reported a tectonic event that led to the formation of eclogite during the subduction of an oceanic lithosphere at around 600 Ma. This could correspond to the zircon population at 620 ± 17 Ma. The younger population (568 ± 11 Ma) represents the climax of the Lufilian orogeny between 560 and 550 Ma, corresponding to the collision of the Congo and Kalahari Cratons (Porada and Berhorst, 2000).

Master et al. (2005) proposed that the maximum sedimentation age for the Biano Subgroup was 573 Ma. This would imply that the Biano Subgroup was deposited before the climax of the Lufilian orogeny. However, the fact that the Biano Subgroup is not deformed suggests that it was deposited during or after the collision of the Congo and Kalahari Cratons. The presence in the Biano Subgroup of sediment clasts from the underlying Katangan rocks also indicates that these rocks were folded before or during its deposition. According to Kampunzu et al. (2003) and Batumike et al. (2006), this folding started before or during the deposition of the Kyandamu Formation (Petit Conglomérat) that represents the Marinoan glaciation in the region, dated at around 620 Ma. Knoll and Walter (1992) and Donnadieu et al. (2004) found that this general Marinoan to Varangian glaciation took place between ∼650 and 565 Ma. This suggests that if the Biano Subgroup was deposited at around 570 Ma, it might contain some features indicative of frigid environments. The absence of any zircons with ages <560 Ma supports the interpretation that the Biano Subgroup was deposited during the Lufilian orogeny, and not afterward.

5.5. *Origin of zircons: basement versus sediment, and crustal evolution*

The zircons analysed in this study were collected in streams crosscutting kimberlite pipes in the Kundelungu Plateau; they are xenocrysts that were collected by the kimberlitic magma during its ascent. The Kundelungu Plateau is constituted of sandstones, limestones and mudrocks belonging to the Biano Subgroup at the top of the Katangan Supergroup, and the nature of the basement beneath this plateau is still controversial. The study of external morphology and internal structure of zircons sampled by the kimberlitic magma provides an opportunity to understand the nature of the basement beneath the plateau.

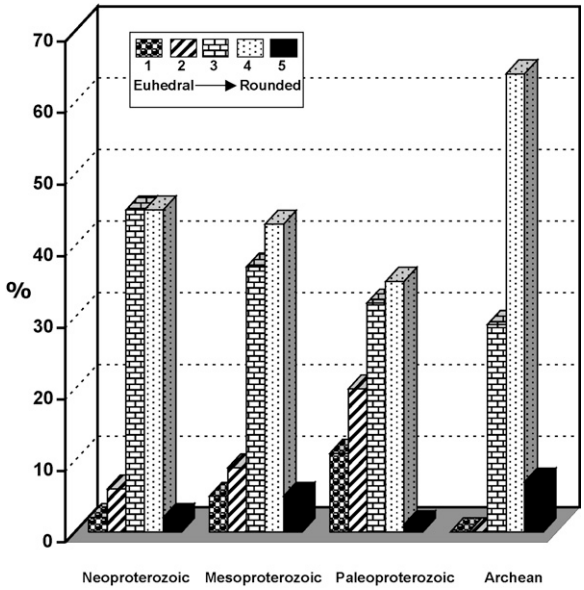

Fig. 9. Relative proportion of different morphological groups of zircon, by age population (Ma).

The analysis of the external morphology of the zircon grains is presented in Fig. 9. The roundness of the zircon grains giving the age of ∼3.3 Ga, and absence of any euhedral grains in the Archean population analysed here, indicate that these grains underwent recycling during transportation and sedimentation. This does not support the extension of an Archean basement beneath the Kundelungu region, as postulated by Rainaud et al. (2005) in the central part of the Lufilian Belt. As argued above, the presence of younger zircons with low Hf-isotope ratios could suggest the presence of an Archean crust during Neoproterozoic time, but the morphology and internal structure of the grains, and the similarity between their $^{176}Hf/^{177}Hf$ initial ratios and those of Paleoproterozoic zircons, make this interpretation ambiguous.

The higher abundance of euhedral zircons, and the lower abundance of rounded zircons, in the Paleoproterozoic population compared to the other age groups (Fig. 9), suggest that a high proportion of this group was derived directly from igneous rocks, rather than from younger sediments. This observation makes the Paleo-

proterozoic Bangweulu Block the best candidate for the basement directly beneath the Kundelungu Plateau. The Mesoproterozoic Kibaran Belt is the next most likely candidate, as the Mesoproterozoic zircon population also contains a relatively high abundance of euhedral zircons. Considering that the Biano Subgroup that hosts the kimberlites in the Kundelungu Plateau is formed of sediments from the Paleoproterozoic Bangweulu Block and the surrounding Mesoproterozoic belts, the recycled zircon grains in the Paleoproterozoic populations could then come from the Biano rocks that were sampled by the kimberlitic magma.

The evolution of the crust in the region is summarised in Fig. 8b. The older Mesoarchean juvenile crust underwent recycling during late-Archean and Paleoproterozoic time. During the Paleoproterozoic there was some input of juvenile material into the crust and the juvenile magmatism was essentially mafic. This Paleoproterozoic crust underwent recycling during events in both Mesoproterozoic and Neoproterozoic time. The important input of juvenile material during late Neoproterozoic time is linked with the breakup of Rodinia around 1 Ga. The juvenile magmatism during Neoproterozoic time (760–690 Ma) corresponds to the opening of the Mwashia basin and the Lufilian orogeny. This episode of juvenile crust formation was followed by crustal reworking until ca. 610 Ma; the last magmatic activity in the region, as recorded in these sediments, involved a new juvenile input at 560–590 Ma.

6. Conclusions

U–Pb and Hf-isotope data on 229 zircon grains from drainages in the Kundelungu Plateau give a good overview on the nature of the basement in the Kundelungu region and the broad crustal evolution in the region, and constrain the provenance of Katangan Supergroup sedimentary rocks. The oldest crust in the region (approximately 3.4 Ga) underwent varying degrees of recycling during Neoarchean and Paleoproterozoic times. Only a very small juvenile input was recognised for the major Paleoproterozoic event but as basaltic additions have low zircon contents, the juvenile input may be underestimated. The bimodal magmatism observed during the Mesoproterozoic (1 Ga) and Neoproterozoic (700–568 Ma) events corresponds to the continental extension and rifting related to the breakup of the Rodinia supercontinent, the opening of the Mwashia basin and the Lufilian orogeny. These periods are also characterised by a large input of juvenile material.

The sediments constituting the Katangan Supergroup were derived from most of the older rocks in the region including the Archean Congo-Kasai, the Paleoproterozoic Ubendian Belt (Bangweulu Block), the Paleo-to-Mesoproterozoic Irumide Belt, the Mesoproterozoic Kibaran Belt and the Choma-Kalomo Block, with a possible minor contribution from the Zimbabwe Craton far south of the Katangan basin. The absence of any zircons with ages <560 Ma suggests that the Biano Subgroup sediments were deposited during the Lufilian orogeny. The basement beneath the Kundelungu region probably consists predominantly of Paleoproterozoic rocks. The rounded morphology of Archean zircons does not support the presence of an Archean crust beneath the Kundelungu Plateau, although Hf-isotope data may be interpreted as evidence that an Archean crust existed at depth during Mesoproterozoic and Neoproterozoic time.

Acknowledgements

This research was supported by an ARC Discovery and Linkage grants (SYO'R and WLG), IPRS (Commonwealth Australia) and iMURS (Macquarie University) scholarships (JMB) and used instrumentation funded by ARC LIEF and DEST Systemic Infrastructure Grants, Macquarie University and Industry. JMB also thanks GEMOC, the Department of Earth and Planetary Sciences (Macquarie University) for research support and fieldwork logistical and financial assistance. Macquarie International provided a contribution to travel for fieldwork. We acknowledge valuable comments and suggestions from B. De Waele, an anonymous reviewer and the editor that helped improve the quality of the manuscript. We thank Norm Pearson and Suzy Elhlou for analytical assistance, and Eloise Beyer for help during data processing. This is contribution 464 from the ARC National Key Centre for the Geochemical Evolution and Metallogeny of Continents (www.es.mq.edu.au/GEMOC).

References

Andersen, T., 2002. Correction of common Pb in U–Pb analyses that do not report ^{204}Pb. Chem. Geol. 192, 59–79.

Barr, M.W.C., Cahen, L., Ledent, D., 1977. Geochronology of syntectonic granites from the central Zambia: Lusaka granite and granite NE of Rufunsa. Ann. Soc. Géol. Belg. 100, 47–54.

Barron, J.W., Broughton, D.W., Armstrong, R.A., Hitzman, M.W., 2003. Petrology, geochemistry and age of gabbroic bodies in the Solwezi area, northwestern Zambia. In: IGCP-450 3rd Conference, Abstr. vol., Lubumbashi, D.R. Congo, pp. 75–77.

Batumike, J.M., Cailteux, J.L.H., Kampunzu, A.B., 2007. Lithostratigraphy, basin development, base metal deposits, and regional correlations of the Neoproterozoic Nguba and Kundelungu rock

successions, central African Copperbelt. Gondwana Res. 11, 432–447.

Batumike, J.M., Kampunzu, A.B., Cailteux, J.L.H., 2006. Petrology and geochemistry of the Neoproterozoic Nguba and Kundelungu Groups, Katanga Supergroup, southeast Congo: implications for provenance, paleoweathering and geotectonic setting. J. Afr. Earth Sci. 44, 97–115.

Belousova, E.A., Griffin, W.L., Shee, S.R., Jackson, S.E., O'Reilly, S.Y., 2001. Two age populations of zircons from the Timber Creek kimberlites, Northern Territory, Australia, as determined by laser ablation-ICPMS analysis. Aust. J. Earth Sci. 48, 757–766.

Belousova, E.A., Walters, S., Griffin, W.L., O'Reilly, S.Y., Fisher, N.I., 2002. Zircon trace-element compositions as indicators of source rock type. Contrib. Miner. Petrol. 143, 602–622.

Binda, P.L., Porada, H., 1995. Observations on the Katangan breccias of Zambia. In: Wendorff, M., Tack, L. (Eds.). Structure and metallogeny of Central African Neoproterozoic belts. Mus. Roy. Afr. Centr., Tervuren, Belgium, Ann. Sci. Géol. 101, 49–62.

Black, L.P., Gulson, B.L., 1978. The age of the Mud Tank carbonatite, Strangways Range Northern Territory. J. Aust. Geol. Geophys. 3, 227–232.

Blichert-Toft, J., Chauvel, C., Albarède, F., 1997. The Lu–Hf geochemistry of chondrites and the evolution of the mantle–crust system. Earth Planet. Sci. Lett. 148, 243–258.

Bulambo, M., De Waele, B., Kampunzu, A.B., Tembo, F., 2004. SHRIMP U–Pb geochronology of the Choma-Kalomo block (Zambia) and geological implications. In: 20th Colloquium of African Geology, Orléans, France, p. 96.

Caen-Vachette, M., Vialette, Y., Bassot, J.P., Vidal, P., 1988. Apport de la géochronologie isotopique à la connaissance de la géologie Gabonaise. Chron. Rech. Min. 491, 35–54.

Cahen, L., Snelling, N.J., Delhal, J., Vail, J.R., 1984. The Geochronology and Evolution of Africa. Claredon Press, Oxford, 512 pp.

Cailteux, J., Binda, P.L., Katekesha, W.M., Kampunzu, A.B., Intiomale, M.M., Kapenda, D., Kaunda, C., Ngongo, K., Tshiauka, T., Wendorff, M., 1994. Lithostratigraphical correlation of the Neoproterozoic Roan Supergroup from Shaba (Zaire) and Zambia, in the central African copper-cobalt metallogenic province. In: Kampunzu, A.B., Lubala, R.T. (Eds.), Neoproteozoic Belts of Zambia, Zaire and Namibia. J. Afr. Earth Sci. 19, 265–278.

Condie, K.C., 2002. Breakup of a Paleoproterozoic Supercontinent. Gondwana Res. 5 (1), 41–43.

Cox, R.A., Rivers, T., Mapani, B., Tembo, T., De Waele, B., 2002. New U–Pb data for the Irumide Belt: LAM-ICP-MS results for Luangwa Terrane. In: Geological Society of Namibia (Ed.), 11th IAGOD Quadrennial Symposium and Geocongress. Windhoek, Namibia, 3 pp.

Delhal, J., Ledent, D., 1973. Résultats de quelques mésures d'âges radiométriques par la méthode Rb/Sr dans les pegmatites de la Haute Luanyi, région du Kasai (Zaïre). Rapp. Ann. Mus. Roy. Afr. Centr. Tervuren, Belgique, Dept. Géol. Min., vol. 1972, pp. 102–103.

Delhal, J., Ledent, D., Torquato, J., 1976. Nouvelles données géochronologiques relatives au complexe gabbro-noritique et charnockitique du bouclier du Kasaï et son prolongement en Angola. Ann. Soc. Géol. Belg. 99, 211–226.

Delhal, J., Liégeois, J.-P., 1982. Le socle granito-gneissique du Shaba occidental (Zaïre): Pétrographie et géochronologie. Ann. Soc. Géol. Belg. 105, 295–301.

De Waele, B., Mapani, B., 2002. Geology and correlation of the central Irumide belt. J. Afr. Earth Sci. 35, 385–397.

De Waele, B., Kampunzu, A.B., Mapani, B.S.E., Tembo, F., 2006a. The Mesoproterozoic Irumide belt of Zambia. J. Afr. Earth Sci. 46, 36–70.

De Waele, B., Liégeois, J.-P., Nemchin, A.A., Tembo, F., 2006b. Isotopic and geochemical evidence of Proterozoic episodic crustal reworking within the Irumide belt of south-central Africa, the southern metacratonic boundary of an Archaean Bangweulu Craton. Prec. Res. 148, 225–256.

De Waele, B., Wingate, M.T.D., Fitzsimons, I.C.W., Mapani, B.S.E., 2003. Untying the Kibaran knot: a reassessment of Mesoproterozoic correlations in southern Africa based on SHRIMP U–Pb data from the Irumide belt. Geology 31, 509–512.

Donnadieu, Y., Goddéris, Y., Ramstein, G., Nédélec, A., Meert, J., 2004. A'snowball Earth' climate triggered by continental break-up through changes in runoff. Nature 428, 303–306.

Fernandez-Alonso, M., Lavreau, J., Klerkx, J., 1986. Geochemistry and geochronology of the Kibaran granites in Burundi, Central Africa: Implications for the Kibaran orogeny. Chem. Geol. 57, 217–234.

François, A., 1973. L'extremité occidentale de l'arc cuprifère shabien. Etude géologique. Dépt. Géol. Gécamines, Likasi, Shaba, Zaïre, 120 pp.

François, A., 1987. Synthèse géologique de l'arc cuprifère du Shaba (Rép. du Zaïre). Centenaire Soc. Belge Géol, pp. 15–65.

Griffin, W.L., Belousova, E.A., Shee, S.R., Pearson, N.J., O'Reilly, S.Y., 2004. Archean crustal evolution in the northern Yilgarn Craton: U–Pb and Hf-isotope evidence from detrital zircons. Prec. Res. 131, 231–282.

Griffin, W.L., Belousova, E.A., Walters, S.G., O'Reilly, S.Y., 2006. Archean and Proterozoic crustal evolution in the eastern succession of the Mt Isa district Australia: U–Pb and Hf-isotope studies of detrital zircons. Aust. J. Earth Sci. 53, 125–149.

Griffin, W.L., Pearson, N.J., Belousova, E.A., O'Reilly, S.Y., Van Achterberg, E., Shee, S.R., 2000. The Hf-isotope composition of cratonic mantle: LAM-MC-ICPMS analysis of zircon megacrysts in kimberlites. Geochem. Cosmochim. Acta 64, 133–147.

Hanson, R.E., Wilson, T.J., Munyanyiwa, H., 1994. Geologic evolution of the Neoproterozoic Zambezi Orogenic Belt in Zambia. J. Afr. Earth Sci. 18, 135–150.

Hanson, R.E., Wilson, T.J., Wardlaw, M.S., 1988. Deformed batholiths in the Neoproterozoic Zambezi Belt Zambia: age and implications for regional Proterozoic tectonics. Geology 16, 1134–1137.

Jackson, S.E., Pearson, N.J., Griffin, W.L., Belousova, E.A., 2004. The application of laser ablation-inductively coupled plasma-mass spectrometry to in situ U–Pb zircon geochronology. Chem. Geol. 211, 47–69.

John, T., Schenk, V., Mezger, K., Fembo, F., 2004. Timing and PT evolution of whiteschist metamorphism in the Lufilian Arc-Zambezi belt Orogen (Zambia): Implications for the assembly of Gondwana. J. Geol. 112, 71–90.

Johnson, S.P., De Waele, B., Liyungu, K.A., 2006. U–Pb sensitive high-resolution ion microprobe (SHRIMP) zircon geochronology of granitoid rocks in eastern Zambia: Terrane subdivision of the Mesoproterozoic Southern Irumide Belt. Tectonics 25, 29 pp (TC6004).

Johnson, S.P., Rivers, T., De Waele, B., 2005. A review of the Mesoproterozoic to early Palaeozoic magmatic and tectonothermal history of south-central Africa: implications for Rodinia and Gondwana. J. Geol. Soc., London 162, 433–450.

Kabengele, M., Lubala, R.T., Cabanis, B., 1991. Caractérisation pétrologique et géochimique du magmatisme ubendien du secteur de Pepa-Lubumba sur le Plateau des Marungu (Nord-est du Shaba,

Zaïre). Signification géodynamique dans l'évolution de la chaîne Ubendienne. J. Afr. Earth Sci. 13 (2), 243–265.

Kampata, M.D., 1993. Minéralogie et géochimie des kimberlites du Haut Plateau de Kundelungu (Shaba, Zaïre). Doc. Thesis. Univ. Cathol. Louvain, 248 pp.

Kampunzu, A.B., Cailteux, J., 1999. Tectonic evolution of the Lufilian Arc (Central Africa Copperbelt) during the Neoproterozoic Pan-African orogenesis. Gondwana Res. 2, 401–421.

Kampunzu, A.B., Cailteux, J.L.H., Batumike, J.M., Loris, N.B.T., 2003. Syn-orogenic sedimentation in the Katangan belt: myth or reality? Multi-proxy constraints. In: Cailteux, J.L.H. (Ed.), Proterozoic sediment-hosted base metals deposits of Western Gondwana (IGCP 450), 3rd conference, Abst. vol. Lubumbashi, Congo, pp. 98–102.

Kampunzu, A.B., Rumvegeri, B.T., Kapenda, D., Lubala, R.T., Caron, J.P., 1986. Le Kibaride d'Afrique centrale et orientale: une chaine de collision. UNESCO, Geol. Econ. Dev., Newslett. 5, 125–137.

Kampunzu, A.B., Tembo, F., Matheis, G., Kapenda, D., Huntsman-Mapila, P., 2000. Geochemistry and tectonic setting of mafic igneous units in the Neoproterozoic Katangan basin, Central Africa: Implications for Rodinia break-up. Gondwana Res. 3 (2), 125–153.

Key, R.M., Liyungu, A.K., Njamu, F.M., Somwe, V., Banda, J., Mosley, P.N., Armstrong, R.A., 2001. The western arm of the Lufilian Arc NW Zambia and its potential for copper mineralization. J. Afr. Earth Sci. 33 (3–4), 503–528.

Klerkx, J., Liégeois, J.-P., Lavreau, J. and Claessens, W. 1987. Crustal evolution of the northern Kibaran Belt, Eastern and Central Africa. In: Kröner, A. (Ed.), Proterozoic lithospheric evolution. Geodynamics Series. Amer. Geophys. Union 17, 217–233.

Knoll, A.H., Walter, M.R., 1992. Latest Proterozoic stratigraphy and Earth history. Nature 356, 673.

Kokonyangi, J., Armstrong, R., Kampunzu, A.B., Yoshida, M., Okudaira, T., 2004. U–Pb zircon geochronology and petrology of granitoids from Mitwaba (Katanga Congo): implications for the evolution of the Mesoproterozoic Kibaran belt. Prec. Res. 132, 79–106.

Kokonyangi, J.W., Kampunzu, A.B., Armstrong, R., Arima, M., Yoshida, M., Okudaira, T., 2007. U–Pb SHRIMP dating of detrital zircons from the Nzilo Group (Kibaran Belt): Implications for the source of sediments and Mesoproterozoic evolution of Central Africa. J. Geol. 115, 99–113.

Kokonyangi, J.W., Kampunzu, A.B., Armstrong, R., Yoshida, M., Okudaira, T., Arima, M., Ngulube, D.A., 2006. The Mesoproterozoic Kibaride belt (Katanga SE D. R. Congo). J. Afr. Earth Sci. 46, 1–35.

Lenoir, J.L., Liégeois, J.-P., Theunissen, K., Klerkx, J., 1994. The Paleoproterozoic Ubendan shear belt in Tanzania: geochronology and structure. J. Afr. Earth Sci. 19 (3), 169–184.

Liyungu, A.K., Mosley, P.N., Njamu, F.M., Banda, J., 2001. Geology of the Mwinilunga area. Rep. Geol. Surv. Zambia 110, 36.

Master, S., 1991. Stratigraphy, tectonic setting, and mineralisation of the early Proterozoic Magondi Supergroup, Zimbabwe: a review. Inf. Circul., EGRU, Dept. Geol., Univ. Witswatersrand, Johannesburg 238, 75 p.

Master, S., Rainaud, C., Armstrong, R.A., Phillips, D., Robb, L.J., 2005. Provenance ages of the Neoproterozoic Katanga Supergroup (Central African Copperbelt), with implications for basin evolution. J. Afr. Earth Sci. 42 (1–5), 41–60.

N'Gambi, O., Boelrijk, N.A.I.M., Priem, H.N.A., Daly, M.C., 1986. Geochronology of the Mkushi Gneiss complex, central Zambia. Prec. Res. 32, 279–295.

Ngoyi, K., Liégeois, J.-P., Demaiffe, D., Dumont, P., 1991. Age tardi-Ubendien (Protérozoique inférieur) des dômes granitiques de l'arc cuprifère zaïro-zambien. C. R. Acad. Sci., Paris 313 (II), 83–89.

O'Reilly, S.Y., Griffin, W.L., Belousova, E.A., 2004. TerraneChron™ delivering a competitive edge in exploration. Ext. Abst. SEG 2004 Centre Glob. Metall., Univ. West. Aust., Publ. 33, 145–148.

Porada, H., Berhorst, V., 2000. Towards a new understanding of the Neoproterozoic-Early Palaeozoic Lufilian and northern Zambezi Belts in Zambia and the Democratic republic of Congo. J. Afr. Earth Sci. 30 (3), 727–771.

Rainaud, C., Armstrong, R.A., Master, S., Robb, L.J., 1999. A fertile Paleoproterozoic magmatic arc beneath the Central African Copperbelt. In: Stanley, C.J. (Ed.), Mineral Deposits: Processes to Processing, vol. 2. Balkema, Rotterdam, pp. 1427–1430.

Rainaud, C., Master, S., Armstrong, R.A., Phillips, D., Robb, L.J., 2005. Monazite U–Pb dating and ^{40}Ar-^{39}Ar thermochronology of metamorphic events in the Central Africa Copperbelt during the Pan-African Lufilian Orogeny. J. Afr. Earth Sci. 42, 183–199.

Rainaud, C., Master, S., Armstrong, R.A., Robb, L.J., 2003. A cryptic Mesoarchean terrane in the basement to the Central African Copperbelt. J. Geol. Soc., London 160, 11–14.

Schildlowski, M., Todt, W., 1998. The Proterozoic Lomangundi carbonate province as a paragon of a ^{13}C-enriched carbonate facies: geology, radiometric age and geochemical significance. Chin. Sci. Bull. 43 (Suppl.), 114.

Shang, C.K., Satir, M., Siebel, W., Nsifa, E.N., Taubald, H., Liégeois, J.-P., Tchoua, F.M., 2004. TTG magmatism in the Congo Craton; a view from major and trace element geochemistry, Rb–Sr and Sm–Nd systematics: case of the Sangmelima region, Ntem complex, southern Cameroon. J. Afr. Earth Sci. 40, 61–79.

Tack, L., Fernandez-Alonso, M., Tahon, A., Wingate, M., Barritt, S., 2002. The "Northeastern Kibaran Belt" (NKB) and its mineralisations reconsidered: New constraints from a revised lithostratigraphy, s GIS-compilation of existing geological maps and a review of recently published as well as unpublished igneous emplacement ages in Burundi. In: 11th IAGOD Quadrennial Symposium, Geocongress. Geological Society of Namibia, Windhoek, Namibia, 6 pp.

Tchameni, R., Mezger, K., Nsifa, N.E., Pouclet, A., 2000. Neoarchean crustal evolution in the Congo Craton: evidence from K rich granitoids of the Ntem Complex, southern Cameroon. J. Afr. Earth Sci. 30 (1), 133–147.

Van Achterbergh, E., Ryan, C.G., Jackson, S.E., Griffin, W.L., 2001. Data reduction software for La-ICP-MS: appendix. In: Sylvester, P.J. (Ed.), Laser Ablation-ICP-Mass Spectrometry in the Earth Sciences: Principles and Applications, vol. 29. Mineralog. Assoc. Canada (MAC) Short Course Series, Ottawa, Ontario, Canada, 239–243.

Vrána, S., Kachlik, V., Kröner, A., Marheine, D., Seifert, A.V., Zacek, V., Baburek, J., 2004. Ubendian basement and its late Mesoproterozoic and early Neoproterozoic structural and metamorphic overprint in the northern Zambia. J. Afr. Earth Sci. 38, 1–21.

Walraven, F., Rumvegeri, B.T., 1993. Implications of whole-rock Pb–Pb and zircon evaporation dates for the early metamorphic history of the Kasai Craton Southern Zaire. J. Afr. Earth. Sci. 16 (4), 395–404.

Wiedenbeck, M., Alle, P., Corfu, F., Griffin, W.L., Meier, M., Oberli, F., Von Quart, A., Roddick, J.C., Spiegel, W., 1995. Three natural zircon standards for U-Th-Pb, Lu-Th, trace element and REE analyses. Geostand. Newslett. 19 (1), 1–23.